Peer-reviewed version available at *Minerals* **2018**, *8*, 594; doi:10.3390/min8120594

Article

The Significant Role of Different Magnesium: Carbonate Minerals Induced by Moderate Halophile *Staphylococcus epidermis* Y2

Zuozhen Han[1, 2*], Wenwen Yu[1], Yanhong Zhao[1], Maurice E. Tucker[4, 5], Huaxiao Yan[3*]

[1] Shandong Provincial Key Laboratory of Depositional Mineralization and Sedimentary Minerals, College of Earth Science and Engineering, University Hospital, Shandong University of Science and Technology, Qingdao, 266590, China

[2] Laboratory for Marine Mineral Resources, Qingdao National Laboratory for Marine Science and Technology, Qingdao, 266237, China

[3] Department of Bioengineering, College of Chemical and Environmental Engineering, Shandong University of Science and Technology, 266590, Qingdao, China

[4] School of Earth Sciences, University of Bristol, Bristol, BS8 1RJ, UK

[5] Cabot Institute, University of Bristol, Cantock's Close, Bristol, BS8 1UJ, UK

✉: Zuozhen Han; Tel.: +86 532 86057286; E-mail: hanzuozhen65@126.com

✉: Huaxiao Yan; Tel.: +86 532 86057625; E-mail: 15954804511@163.com

Abstract: Carbonate precipitation induced by microorganism has become a hot spot in the field of carbonate sedimentology, while the effect of different magnesium on biominerals has rarely been studied. Therefore, magnesium sulfate and magnesium chloride were used to investigate the significant role played on carbonate minerals. In this study, *Staphylococcus epidermidis* Y2 was isolated and identified by 16S rDNA homology comparison. The ammonia, pH, carbonic anhydrase, carbonate and bicarbonate ions were investigated. The mineral phase, morphology and elemental composition were analyzed by XRD and SEM-EDS. The ultrathin slices of bacteria were analyzed by HRTEM-SAED and STEM. The result showed that this bacterium could release ammonia and carbonic anhydrase to increase pH, and elevate the supersaturation via a large number of carbonate and bicarbonate ions released through carbon dioxide hydration catalyzed by carbonic anhydrase. The crystal cell density of monohydrocalcite was lower in magnesium chloride medium than that in magnesium sulfate medium. The crystal grew in a mode of spiral staircas in magnesium sulfate medium, while in a concentric circular pattern in magnesium chloride medium. There was no obvious intracellular biomineralization. This study may be helpful to further understand the biomineralization mechanism, may also provide some references for the reconstruction of paleogeological environment.

Keywords: Moderate halophile; Carbonate minerals; Mg/Ca ratios; Different magnesium, Carbonic anhydrase; pH increase; Cell density; Growth mode

1. Introduction

As an important reservoir of oil and gas, carbonate rock has drawn much attention in recent years [1-4]. Subsequently microbial fossils have been found in carbonate rocks, and people have just realized the existence of microbialites. The microbialites are an important part of carbonate rocks and widely distributed in the ocean and lake environment [5-9]. Stromatolites, thrombolites, dendrites and leiolites are very common microbialites [10-14]. Biomineralization researches have proved that the microorganisms have played a significant role in the microbialite formation, which has changed the view that the formation of microbialites are mainly caused by some physical and chemical factors [15-18]. Thus, there is a close relationship between the microorganisms and the carbonate precipitation, which has also become a research hot spot in the field of geomicrobiology and sedimentology [19]. Based on the conclusion that the formation of microbialites is related to the

microorganisms, many researchers have carried out the experimental research on the formation of carbonate minerals induced by various microorganisms in the laboratory and natural environment in order to explore the mechanism of biomineralization more deeply and get more innovative conclusions [20,21]. The research of microbial biomineralization has indeed made great progress in the past few years [22,23].

Microorganisms that have been reported to be able to induce the precipitation of the carbonate minerals include cyanobacteria [24-27], alkalophilic and halophilic microorganisms [28-31], sulfate-reducing bacteria [32-34], methanogenic archaea [35-38], and other bacteria like bacillus [29] and so on. It has been reported that the primitive life on Earth may originate from the high salt environment [39,40]. Some researchers have also analyzed the dolomite and limestone in the nature and concluded that the palaeogeologic environments used to form these carbonate rocks were the seas [41-43], which were also the salt environments. Therefore, the study of the viability and adaptability of microorganisms in modern salt environment will help to deeply understand the evolution of biosphere in the early Earth. In the field of geomicrobiology, screening salt-tolerant halophilic bacteria to induce the carbonate minerals at a certain salt concentration is helpful to analyze the formation mechanism of microbialites in the past [7,44-48]. Many geologists have used halophilic bacteria to induce the precipitation of carbonate minerals in the laboratory, which have also proved that there is a close relationship between the halophilic bacteria and the formation of carbonate minerals and also further testify the close connection between lithosphere and biosphere. Rivadeneyra et al. [49,50] have studied the deposition of carbonate by *Halmonas eurihalina* and *Nesterenkonia halobia* and their results have showed that the precipitated minerals by the former bacteria are magnesium calcite, aragonite and monohydrocalcite, and the minerals induced by the latter bacteria are calcite, aragonite and dolomite, and also revealed that the proportion of various minerals is related to the type and salt concentration of the culture medium and the cultivation time. The halophilic bacteria isolated from soil by Párraga et al. [51] can induce the formation of calcite pellets with a diameter of 20 to 50 μm, which are considered to play a positive role in calcite deposition in saline soils. Sánchez-Román et al. [30] have used 19 kinds of moderate halophilic bacteria to precipitate the carbonate and phosphate minerals in the culture medium with controllable Mg/Ca molar ratios, and the minerals deposited are calcite, magnesium calcite and struvite ($MgNH_4PO_4 \cdot 6H_2O$), the proportion of minerals depends on the Mg/Ca ratio in the medium. Studies have also shown that Mg^{2+} can influence the formation of carbonate minerals and more researchers have explored the effect of Mg^{2+} on the mineral morphology and nucleation when using microorganism to induce biomineralization [52-54]. Many researchers have also studied the formation mechanism of modern dolomite by using halophilic bacteria. For example, Qiu et al. [55] have used *Haloferax volcanii* DS52, a halophilic archaeon, to induce the dolomite precipitation under various salinities (from 120 h to 360 h) and restated the important effect of high concentration of salt on the formation of microbiogenic dolomite. Qiu et al. [56] have also concluded that extracellular polymers (EPS) of living cells can chelate calcium and magnesium ions, which can maintain a higher ratio of magnesium and calcium ions around the cell surface to facilitate the formation of carbonate minerals. Deng et al. [57] have isolated the aerobic halophilic bacterium *Halomonas marina* existing in the Qinghai Lake sediments, which can precipitate dolomite in low-salinity conditions without any marine influence. Although there have been many studies on the induction of carbonate minerals by halophilic bacteria, many questions remain unclear and need further exploration.

In the study of carbonate mineral precipitation induced by halophilic bacteria [30,58,59], we have found that there are some different opinions on certain questions. For example, many researchers have performed the ammonia test to determine whether some bacteria can release ammonia, and concluded that the pH increase in the culture medium was due to the ammonia released by bacteria only from the positive result of the ammonia test [30,60,61]. This idea has been accepted by almost researchers for many years. The result of causing pH increase by the ammonia has always been cited by many published papers without any hesitation, even on the condition that we have not performed the experiment to investigate why pH can increase. However, there have been different opinions on the reason of pH increase recently. Some researchers have believed that

the bacteria cannot produce enough ammonia to make pH increase to nearly 9 [62], there should be other factors to influence pH increase. Based on the fact that cyanobacteria can secret carobonic anhydrase (CA), which can promote the hydration reaction of carbon dioxide to release a large number of bicarbonate and carbonate ions to make pH increase [63]. Zhuang et al. [62] have found that CA can also be secreted by the isolated bacteria and can also produce a great number of bicarbonate and carbonate ions. Thus, Zhuang et al. [62] have believed that pH increase is caused by the ammonia and CA. Besides of this, CA catalyzes the hydration of carbon dioxide to produce large amounts of carbonate and bicarbonate, which not only increases the pH but also helps to elevate the supersaturation of some carbonate minerals to promote the precipitation of minerals in the culture medium. Without CA, the rate of producing the bicarbonate and carbonate ions is very slowly [64]; if there is CA, the typical catalytic rate can reach up to 10^4-10^6/s [65]. There are fewer references published to report the precipitation of minerals was closely related to CA activity [66,67]. It has been reported that the composition of the solution and the concentrations of ions have a significant impact on mineral precipitation [29]. Thus, besides of CA, many researchers have mentioned and investigated the significant role played by different Mg/Ca molar ratio in the formation of carbonate minerals, while always neglected the role of different sources of magnesium. The experiment using different sources of magnesium ions to form the carbonate minerals conforms to the different sedimentary environments in geological history [68,69]. In fact, different sources of magnesium used are also important and also have a significant role in the morphology and mineralogy of carbonate minerals in the biomineralization process, however, has rarely been reported. Li et al. [29] have reported the minerals induced by halophilic bacteria with different sources of magnesium, however, they have not investigated the growth way of minerals and also not determined the element distribution on/in the EPS/surface and inside the cell by scanning transmission electron microscopy (STEM) and also not analyzed the amino acid composition of bacterial EPS to further explore the nucleation mechanism. At the same time, many researchers have focused on the extracellular biomineralization and neglect the intracellular biomineralization [70,71]. There are only fewer references reported about the intracellular biomineralizaiton. Benzerara et al. [27] have studied the intracellular biomineralization of cyanobacteria and found that there are amorphous carbonate inclusions inside the cell, but their research is aimed at the cyanobacteria. Zhuang et al. [62] have also found that there are amorphous nanospheres inside the cells, however, the bacteria used to perform the experiment is alkali-tolerant bacteria *Bacillus cereus* MRR2, not the halophilic bacteria. Perri et al. [72] have also reported that nanospheres with a diameter of a few tens of nanometres can also be found within their cells and believed that these nanospheres are maybe permineralized viruses and act as nuclei for the precipitation of crystallite-crystal. Besides of the intracellular biomineralization, there are still many unsolved problems in the biomineralization field, such as the detailed molecular biomineralization mechanism, the true reason of pH increase, the criterion for judging biogenesis of carbonate minerals and so on, which results in the fact that the study of biomineralization still needs further exploration. In our study, we have further studied the precipitation of carbonate minerals induced by halophilic bacteria by using different sources of magnesium to further investigate the role played by different magnesium on the growth way and mineralogy, also studied the role of CA, amino acid composition of EPS, the nucleation site, the element distribution, and the intracellular biomineralization.

In order to further explore the biomineralization mechanism of carbonate minerals induced by halophilic bacteria, experiments were performed by using magnesium chloride and magnesium sulfate, different Mg/Ca molar ratios, 10% sodium choride, and halophilic bacteria *Staphylococcus epidermidis* Y2 which was isolated and identified by 16S rDNA homology analysis. The ammonia, CA activity, the concentration of bicarbonate and carbonate ions, and the amino acid composition of EPS were also analyzed respectively in order to further understand the biomineralization mechanism. The characteristics of carbonate minerals, such as the morphology, elemental composition and mineralogy, were analyzed by means of scanning electron microscope (SEM), energy dispersive spectrometer (EDS) and X-ray powder diffraction (XRD). The superthin slices of

Peer-reviewed version available at Minerals 2018, 8, 594; doi:10.3390/min8120594

S. epidermidis Y2 were also prepared to further analyze the nucleation site on EPS/surface, the distribution of calcium and magnesium elements outside and inside the cell and whether the intracellular nanospheres have crystal structures by high resolution transmission electron microscopy (HRTEM) and selected area electron diffraction (SAED) and STEM. This study may further elucidate the detailed biomineralization mechanism induced by *S. epidermidis* Y2, and also provide some theoretical basis for reconstruction of ancient geological environment.

2 Materials and Methods

2.1. Isolation and Preservation of S. epidermidis Y2 Bacteria

A liquid enrichment culture medium with the following composition was used (g L^{-1}): beef extract 5.0, tryptone 10.0, and NaCl 100. The above reagents were all dissolved in the deionized water and the pH of the culture medium was adjusted to 7.2. The solid medium was prepared by adding 20 g L^{-1} agar powder into the above liquid culture medium. All mediums were sterilized by an autosterilizer at 110 °C for 25 min. The liquid culture medium and the solid culture medium were used to isolate and purify the halophilic bacteria [29]. Y2 bacteria were isolated from pickles purchased from supermarkets. Ten g of pickles were cut into small pieces and inoculated into liquid medium for 7 days of enrichment culture in a constant temperature shaker (HZQ-F160, Harbin Donglian Electronic Technology Development Co., Ltd, China) with a speed of 110 rpm at 30 °C. The phenomenon that the medium became turbid could prove the presence of halophilic bacteria. After the enrichment cultivation, there would be existing a large number of different species of bacteria, if we wanted to obtain a purified bacterium, the next step needed to do was that the bacteria were purified by solid-liquid alternate culture. Twenty μL of 10^{-1}, 10^{-2}, 10^{-3}, 10^{-4}, 10^{-5}-fold diluent of the bacterial liquid culture medium was spread on the surface of the solid culture medium and cultivated for 2 days in a constant temperature incubator (DHP-9050B, Shanghai Langgan Laboratory Equipment Co., Ltd, China) until the single colony could be observed by the naked eye. A single colony was selected to inoculate into the liquid culture medium and cultivated for 24 h in a constant temperature shaker with a speed of 110 rpm at 30 °C, and then the liquid bacterial culture medium was diluted and the above process was performed again. A purified bacterium can be obtained by 3 cycles of solid-liquid process.

The concentration of liquid culture medium containing pure Y2 bacteria was measured by a spectrophotometer (722s, Shanghai Precision and Scientific Instrument Corporation, China) at a wavelength of 600 nm. Only the OD_{600} value reached up to 1.0 could the above liquid culture medium containing pure Y2 bacteria be called the liquid seed and be preserved by 30% sterilized glycerin (v:v) according to a ratio of 1:1(v:v). And then, the preserved Y2 bacteria were stored at -20 °C.

2.2. 16S rDNA Identification of S. epidermidis Y2 Bacteria

A purified bacterium was sent to Bioengineering co., Ltd. (Shanghai, China) for 16S rDNA sequencing, and 16S rDNA splicing was processed by using DNAMAN software [63]. The complete 16S rDNA sequence of Y2 bacteria was uploaded into the GenBank/NCBI database and an accession number could be obtained. The identity between 16S rDNA sequence of Y2 and those of other bacteria preserved in the GenBank/NCBI database could also be obtained by Blast analysis. Phylogenetic tree of Y2 bacterium could be constructed by neighbor-joining method in MEGA 7 software [68].

2.3. Qualitative Test of Ammonia Released by S. epidermidis Y2 Bacteria

The culture medium used to test the presence of ammonia was composed by the following components: peptone 0.5%, K_2HPO_4 0.05%, $MgSO_4$ 0.05%. The pH of this kind of culture medium was adjusted to 7.0 ~ 7.2. And then the Nessler's reagent was prepared by mixing a solution (KI 10 g, HgI 20 g, and distilled water 100 mL) and B solution (KOH 20 g, distilled water 100 mL) and stored in a brown bottle. After that, two tubes inoculated with 10 mL of the above culture medium

Peer-reviewed version available at Minerals 2018, 8, 594; doi:10.3390/min8120594

were prepared, one inoculated with 100 μL of the liquid seed was set as the experimental group and the other inoculated with the same volume of sterilized distilled water was set as the control group. After being cultivated for 24 – 48 h at 30 °C, 3 to 5 drops of Nessler's reagent were added to the two tubes to observe the color changes. If the experimental group showed a dark yellow (or brownish red), the result of ammonia test was positive; if a light yellow, which was the color of Nessler's reagent, the result was negative.

2.4. Growth Curve of S. epidermidis Y2 Bacteria and pH Changes in the Culture Medium

To determine the optimal salt concentration of *S. epidermidis Y2* bacteria, *S. epidermidis Y2* bacteria were inoculated into culture medium with 5%, 10%, 15%, 20%, 25% and 30% sodium chloride at 10% volume ratio, after being cultivated for 24 h in a constant temperature shaker with a speed of 150 rpm at 30 °C, the concentration of *S. epidermidis Y2* bacteria was measured by a spectrophotometer at 600nm. The optimal salt concentration for *S. epidermidis Y2* bacteria was determined by the highest cell concentration.

The liquid seed was inoculated into the liquid culture medium at a volume ratio of 1% and fermented in a constant temperature shaker with a speed of 150 rpm at 30 °C. Three mL of the fermentation liquid was taken out and the cell concentration was measured by a spectrophotometer at 600nm at certain time. With time as the abscissa and cell concentration as the ordinate, the growth curve of *S. epidermidis Y2 bacteria* could be drawn. The pH value of fermented liquid was measured by a pH meter (PHS-3, Jiangsu Jiangfen Instrument and Equipment Company, China) at certain time. With time as the abscissa and pH value as the ordinate, the pH curve of *S. epidermidis Y2 bacteria* could be obtained.

To determine the effect of carbonate ions released by CA on pH increase, pH values could be calculated according to the concentration of carbonate ions if there was only first-order reaction. The concentration of carbonate ions in the liquid culture medium was measured as shown in part 2.6. Therefore, pH curve based on carbonate ion concentration could be obtained.

2.5. Activity of CA Released by S. epidermidis Y2 Bacteria

CA activity was measured according to the modified method described by zhuang et al. [62] respectively. First, phosphate buffer (0.2 M, pH 6.8) was prepared by mixing 250 mL of KH_2PO_4 solution (0.2 M) with 118 mL of NaOH solution (0.2 M), and adding deionized water to a volume of 1 L. The pH of phosphate buffer was adjusted to 6.8 by using hydrochloric acid solution (1 M). One mM of *p*-nitrophenol standard solution was prepared by dissolving 0.0139 g of *p*-nitrophenol into 100 mL of phosphate buffer. Solution A was prepared by dissolving 0.0181 g of *p*-nitrophenyl acetate into 0.5 mL of anhydrous ethanol; solution B was prepared by dissolving 0.156 g of diethyl diethylmalonate diethyl into 99.5 mL phosphate buffer; the working liquid could be obtained by mixing solution A and solution B. The standard solution with a volume of 0.35, 0.3, 0.25, 0.2, 0.15, 0.1, 0.05 and 0 mL was added into a 4-mL centrifuge tube, respectively, then deionized water was added up to 3 mL, and at last the OD value of mixture was measured by a spectrophotometer at a wavelength of 400 nm. Taking the concentration as abscissa and the OD value as ordinate, a stand curve could be obtained. The determination of CA activity was as follows: the bacterial fermented liquid was mixed with the working liquid at a volume ratio of 1: 1, the absorbance of mixture was measured at a wavelength of 400 nm by a spectrophotometer, and then the mixture was placed in a water bath at 35 °C for 30 min, quickly transferred to an icy bath to inactivate the enzyme, after that, the absorbance of mixture was measured again at the same wavelength. The activity of CA enzyme could be calculated according to the above standard equation and the obtained optical absorption value.

2.6. Determination of the Concentration of CO_3^{2-} and HCO_3^- Ions

The concentrations of carbonate and bicarbonate ions in the fermented liquid were measured according to the method described by zhuang et al. [62].

2.7. Amino Acid Composition of EPS

EPS of *S. epidermidis* Y2 bacteria were extracted by heating method according to the reference reported by Morgan et al. [73]. Fermented liquid (OD_{600}=1.0) was centrifuged at 2000 rpm for 10 min. Then, the supernatant was discarded and deionized water was added to the original volume. The mixture was centrifuged again at 2000 rpm for 3 min. In order to wash the cells thoroughly, the above process was repeated twice. The above bacterial suspension was put in a water bath at 60 °C for 30 min, centrifuged at 10000 rpm for 10 min to obtain the supernatant, and then the supernatant was filtered by 0.22 μm-pore sized filter membrane. The obtained colorless transparent EPS solution was dried in a lyophilizer (FD-1A-50, Shanghai Bilang instrument Manufacturing Co. Ltd., China) at – 60 °C. Finally, the dried EPS powder was sent to Jiangsu coast chemical analysis technology service co., LTD., and the amino acid composition of EPS was analyzed by an amino acid analyzer (Hitachi L-8900, Japan).

2.8. Carbonate Minerals Induced by S. epidermidis Y2 Bacteria with Different Sources of Magnesium

In the culture medium used to induce the carbonate minerals, Ca^{2+} ion concentration was 0.01 M, and Mg/Ca molar ratio was set as 0, 2, 4, 6, and 8. Mg^{2+} ions were from two different magnesium sources, namely $MgSO_4$ and $MgCl_2$. The culture medium was sterilized at 121 °C for 30 min. $NaHCO_3$ (1 M) and Na_2CO_3 (1 M) solution was sterilized by a sterilized filter with sterilized 0.22 μm-pore sized membrane. 6 mL of $NaHCO_3$ solution and 3 mL of Na_2CO_3 solution were added into 150 mL of culture medium, respectively. The pH of culture medium was adjusted to 7.2. The liquid seed was inoculated into the culture medium with different sources of Mg^{2+} ions at a volume ratio of 1%, and then was incubated in a constant temperature shaker at 110 rpm and 30 °C.

2.9. Analysis of Carbonate Mineral Induced by S. epidermidis Y2 in $MgSO_4$ Group and $MgCl_2$ Group

In order to determine the difference in the mineralogy of carbonate minerals between $MgSO_4$ group and $MgCl_2$ group, the minerals in $MgSO_4$ group and $MgCl_2$ group were analyzed by XRD (D/Max-RC, Rigaku, Japan) with the scanning angle from 10 ° to 80 °, a step size of 0.02 and a count of 8 °/min [74-80]. The microscopic morphology, size and elemental composition of mineral in $MgSO_4$ group and $MgCl_2$ group were studied by SEM (Hitachi S-4800, Japan) and EDS (EDAX, America) [81-84], respectively. Minerals soaked in anhydrous ethanol were transferred to an aluminum support and dried naturally, and then sprayed with platinum (Pt) powder and analyzed by SEM-EDS [83,85-87].

2.10. Analysis of the Nano-meter Spheres and Element Distribution Outside and Inside of S. epidermidis Y2 Cell

In the process of biomineralization of carbonate minerals, 10 mL of *S. epidermidis* Y2 bacterial liquid was centrifuged at a speed of 3000 rpm for 5 min, the pellet including the minerals and the bacteria was washed 3 times with phosphate buffer ($Na_2HPO_4 \cdot 12H_2O$ 20.7472 g L^{-1}, $NaH_2PO_4 \cdot 2H_2O$ 3.1167 g L^{-1}, pH 7.2) to remove the ingredients from the culture medium. The pellet was fixed by glutaraldehyde (2.5%, v : v) for a night, then dehydrated gradually by acetone solution: 30% (15 min) -50% (15 min) -70% (15 min) -80% (15 min) -90% (15 min) -95% (15 min) -100% (15 min) -100% (15 min) -100% (15 min), at last 30% epoxy resin solution was added to embed the cells. The completed ultra-thin slices were analyzed with TEM (JEM-2100, Japan) [81,88-91], HRTEM (H-7650, Hitachi, Japan) [87,92-94], SAED [86] and STEM (Tecnai G2 F20, FEI, America) [95].

Preprints (www.preprints.org) | NOT PEER-REVIEWED | Posted: 2 November 2018 doi:10.20944/preprints201811.0064.v1

Peer-reviewed version available at Minerals 2018, 8, 594; doi:10.3390/min8120594

3. Results

3.1 Identification of S. epidermidis Y2 Bacteria

The 16S rDNA sequence of *S. epidermidis* Y2 strain uploaded to GenBank (accession number MG725753.1) is 1405 bp long. The 16S rDNA of *S. epidermidis* Y2 strain shares 99 % homology with 99 strains of *S. epidermidis* bacteria by Blast in Genbank. A phylogenetic tree of *S. epidermidis* Y2 bacteria shown in **Fig. 1** indicates that Y2 strain has the closest genetic relationship with *S. epidermidis* species. Therefore, Y2 strain belongs to a species of *S. epidermidis*.

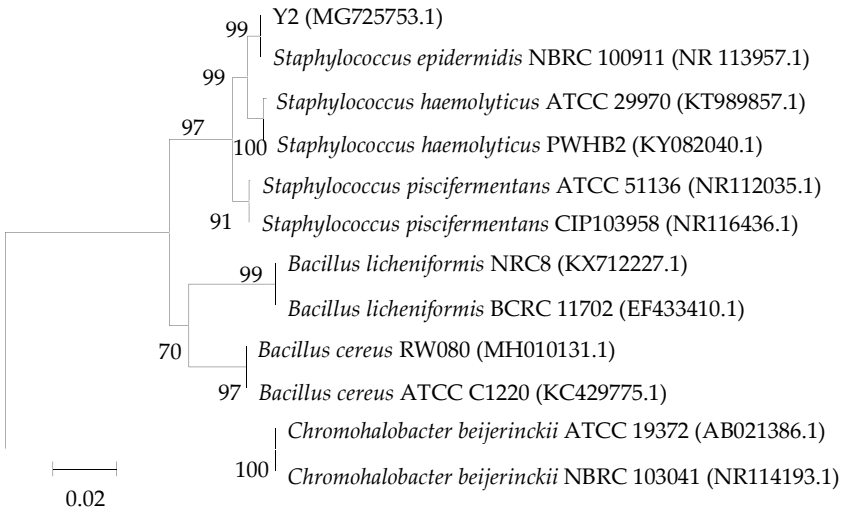

Figure 1. Phylogenetic tree of *S. epidermidis* Y2 based on the sequence alignment.

3.2 Ammonia Qualitative Experiment

After 7 days of culture on an agar plate, a single colony with a diameter of 2-3 mm was formed. The white colonies show a round convex shape, tidy edges, and smooth and moist surface (**Fig. 2a**).

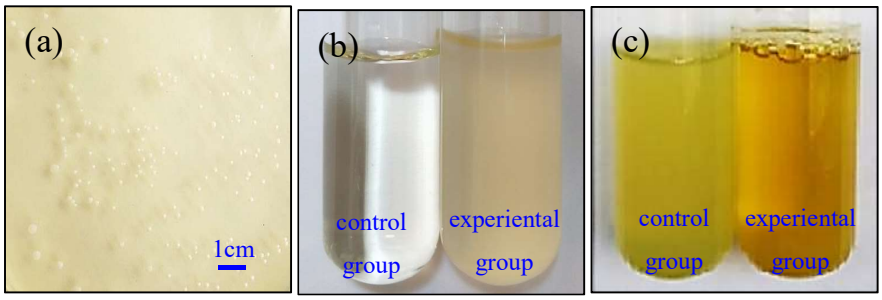

Figure 2. The colony morphology and the ammonia test of *S.epidemidis* Y2 strain
(a), the colony morphology of *S. epidemidis* Y2; (b), the color before adding Nessler reagent; (c), the color after adding Nessler reagent. Dark yellow or brown shows the ammonia test result is positive. Light yellow shows the color of Nessler reagent. The ammonia test shows that ammonia can be released by *S.epidemidis* Y2 strain.

Before adding Nessler reagent, the control group is clear and transparent, and the experimental group is turbid due to the existence of *S. epidermidis* Y2 bacteria (**Fig. 2b**); after adding Nessler reagent, the control group shows a yellow color, which was the original color of Nessler reagent, and the experimental group is brown, different from the original color of the experimental group and the color of Nessler reagent (**Fig. 2c**). The ammonia test result shows that ammonia could be released by *S. epidermidis* Y2 bacteria. That is to say, *S. epidermidis* Y2 bacteria could make full use of amino acids coming from the organic compound such as beef extract and tryptone in the culture medium by transamination and deamination to produce a certain amount of ammonia gas.

The released ammonia can dissolve into the liquid culture medium to produce a large number of hydroxyl ions. The chemical reaction occurred according to the following equation (1):

$$NH_3+H_2O \rightarrow NH_4^+ + OH^- \quad (1)$$

The produced hydroxyl ions can increase pH values of the culture medium, providing favorable conditions for the sedimentation of carbonate minerals.

3.3 Growth Curve and pH Curve of S. epidermidis Y2

Fig. 3a shows the growth curve of *S. epidermidis* Y2 bacteria under different salt concentration. It can be obtained from **Fig. 3a** that the optimum salt concentration for bacterial growth is 10%, the optimum range of salt concentration is 5%-15%, and there are almost no bacteria at 30% salt concentration. That is to say, *S. epidermidis* Y2 bacteria belong to the moderate halophile, not the extreme halophile. In order to explore the relationship between the growth of *S. epidermidis* Y2 bacteria and the increasing pH value in the liquid culture medium, growth curve and pH value curve was studied.

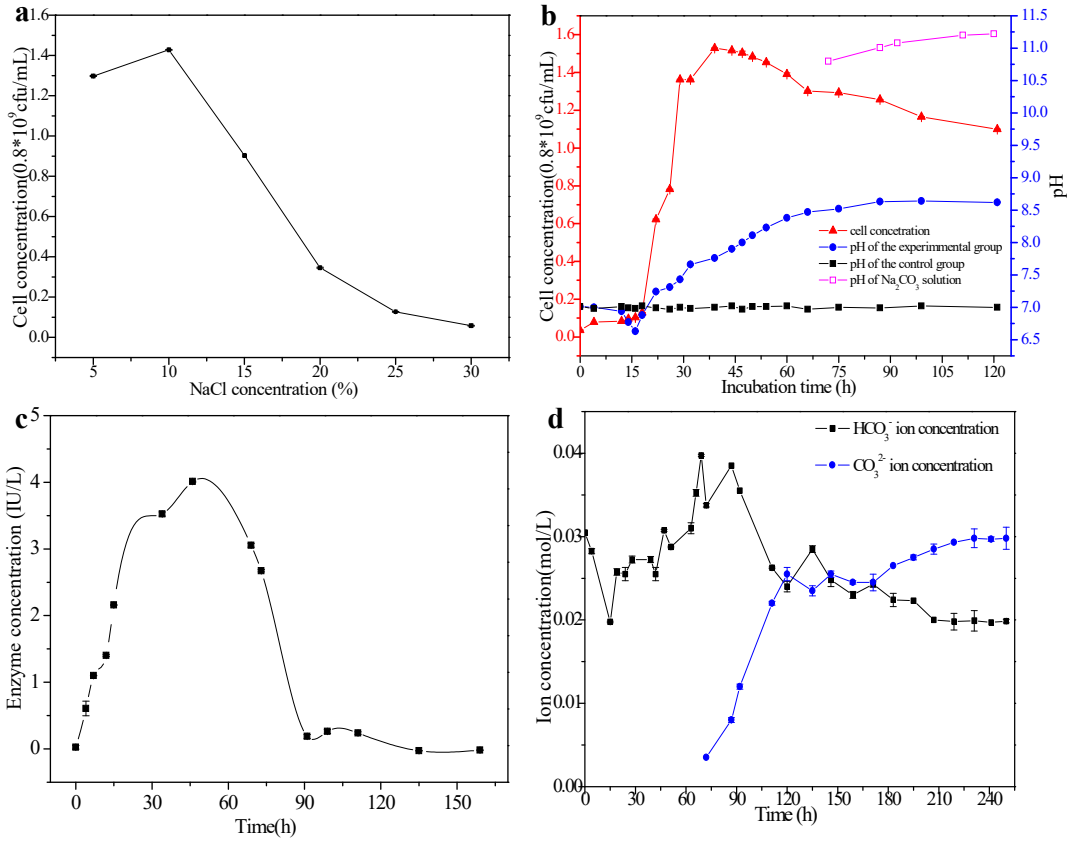

Figure 3. Physiological and biochemical characteristics of *S.epidemidis* Y2 bacteria.
(a) Growth curve of *S.epidemidis* Y2 bacteria at different sodium chloride concentration after being cultivated for 24 h; (b) Growth curve and pH curve; (c), CA activity; (d), Carbonate and bicarbonate ion concentrations in the culture medium.

As shown in **Fig. 3b**, the growth of *S. epidermidis* Y2 can be divided into four main phases: delay (adaption) phase, logarithmic growth phase, stationary phase and delay phase. The time range of 0-18h belongs to the adaption phase, in this period, there is almost no changes in the concentration of *S. epidermidis* Y2 bacterial cells and only little decrease in pH values of the liquid culture medium; the exponential growth period is in a time range of 18-37h, indicating that there was a sharp increase in bacterial concentration, in this period, pH values increased to nearly 8.0 due to the ammonia released by *S. epidermidis* Y2 bacteria; the third stage is stable phase in a time range

Peer-reviewed version available at Minerals 2018, 8, 594; doi:10.3390/min8120594

of 37-44h, the cell concentration of *S. epidermidis* Y2 bacteria is almost unchanged, while, pH still increases; the last stage is decline phase from 44-123h, the cell concentration decreases due to the fact that the large consumption of nutrients leads to the shortage of carbon and nitrogen sources and then limits the proliferation of bacteria [96], also indicating that some metabolic activities of *S. epidermidis* Y2 bacteria also declined, however, pH values still increase from 8.0 to 8.7. **Fig. 3b** also shows that there is a great difference in pH value between the control group and the experimental group. The experimental group can make pH increase to 8.70 with the extension of incubation time, creating an alkaline environment for the precipitation of carbonate minerals. However, pH value in the control group was almost unchanged and kept at 7.0 or so. The significant difference reveals the important role played by *S. epidermidis* Y2 bacteria in pH increase which can help to elevate the alkalinity in the culture medium, also suggesting that *S. epidermidis* Y2 bacteria plays an important role in biomineralization.

3.4 Determination of CA Activity

It has been reported that CA coming from the microorganisms and bovine can promote Ca^{2+} precipitation in the biomineralization process [66,97,98] due to the fact that CA can catalyze the hydration of carbon dioxide to release a large number of bicarbonate and carbonate ions to further elevate the supersaturation of the carbonate minerals. Thus, CA activity of *S. epidermidis* Y2 bacteria was also investigated in this study. CA activity of *S. epidermidis* Y2 bacteria is shown in **Fig. 3c**. The result shows that this bacterium can produce CA and its activity can reach up to a peak (4 IU/L) in the time range of 30-75h and become very low after 90h. The change in CA activity coincides with that of the growth curve, indicating that CA released from *S. epidermidis* Y2 bacteria belongs to the synchronic synthesized enzyme or the growth-coupled type. That is to say, CA activity can increase with the increase of cell concentration of *S. epidermidis* Y2 bacteria, and also decrease correspondingly with the aging of *S. epidermidis* Y2 bacteria.

3.5. Determination of Carbonate and Bicarbonate Ions in the Liquid Culture Medium

The concentration of carbonate and bicarbonate ion was also investigated in this study. **Fig. 3d** shows the changes of bicarbonate and carbonate ion concentration in the liquid culture medium. It can be seen from **Fig. 3d** that the concentration of bicarbonate increases in the time range of 0-69 h that CA activity is high, and decreases rapidly from 69 to 120 h, and then decreased slowly after 120 h; the carbonate ion concentration increases sharply from 69 to 120 h, in the first 69 h, the carbonate ion does not show up, and after 69 h, the carbonate ion begins to appear. With the decrease of the bicarbonate, the carbonate rises. Therefore, in the later stage, the concentration of bicarbonate decreases to 0.01 M or so and while the concentration of carbonate increases to above 0.03 M.

According to carbonate ion concentration, the mass of sodium carbonate can be calculated (Table 1); thus, pH based on carbonate ion concentration could be obtained by measuring the pH value of sodium carbonate solution (Table 1, Fig. 2b). Therefore, a pH curve in Fig. 2b shows that pH value is higher than that in the experimental group. We have concluded that pH increase in the experimental group was also related to the carbonate ions released by CA, not only ammonia released by *S. epidermidis* Y2 bacteria.

3.6. Amino Acid Compositions of EPS

In order to further explore the biomineralization mechanism, EPS were extracted from *S. epidermidis* Y2 bacteria and then the amino acid composition of EPS was analyzed. It can be seen from **Fig. 4** that 17 kinds of amino acids are obtained in this study, and other amino acids are not detected maybe due to the negligible content. The content of glycine (Gly) is the highest among all these amino acids, the molar ratio of alanine (Ala) and proline (Pro) is less than that of Gly, glutamic acid (Glu) and aspartic acid (Asp) are acidic amino acids and the contents of Asp and Glu are next to those of Gly, Ala and Pro. The contents of basic amino acids such as lysine (Lys), arginine (Arg) and histidine (His) are far less than those of acidic amino acids. *S. epidermidis* Y2 bacteria belong to

mederate halophile and can tolerate a certain osmosis environment caused by the presence of high concentration of sodium choride. The special ability of *S. epidermidis* Y2 bacteria to tolerate high

Table 1 The pH of Na_2CO_3 Solution from 72h to 120 h

Time(h)	CO_3^{2-} (mol / L)	Na_2CO_3 (g / 100 mL)	pH
72	0.0035	0.0371	10.80
87	0.008	0.0848	11.01
92	0.012	0.1272	11.08
111	0.022	0.2332	11.20
120	0.0255	0.2703	11.22

concentration of sodium choride has a close relationship with the components and structures of EPS. It has been reported that Gly can be transformed into betaine by methylation reactions catalyzed by methyltransferases, and betaine accumulation can improve salt tolerance of the heterologous organisms [99]. In this study, moderate halophile *S. epidermidis* Y2 bacteria can tolerate 10% sodium choride may be due to the abundant of Gly. There are four groups in Gly: two hydrogen atoms, NH_2- group and COO^- group. NH_2- group and COO^- group can form peptide bond and two hydrogen atoms are free, thus EPS rich in Gly have some certain hydrophobicity. This property has the effect of preventing salt ions from entering the cell, and has a protective effect on *S. epidermidis* Y2 bacterial cell.

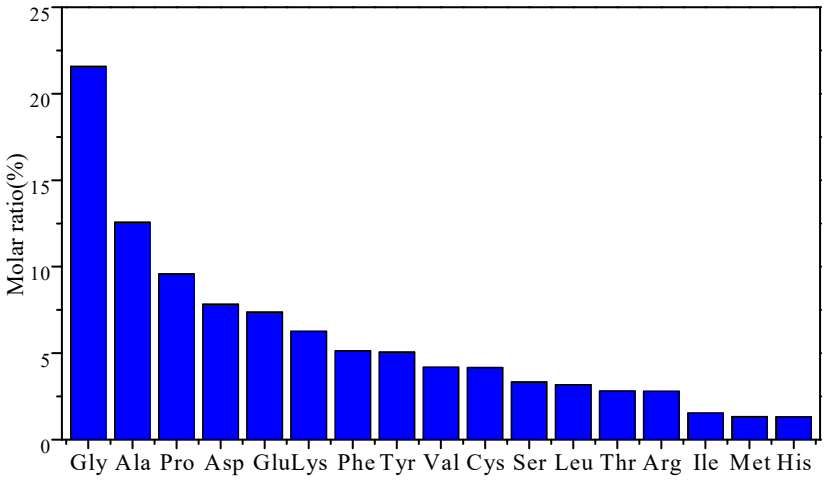

Figure 4. The amino acid composition of EPS from *S. epidermidis* Y2

3.7 XRD Analysis of Minerals in the Culture Medium with Different Sources of Magnesium

To further study what different kinds of minerals can be induced by the moderate halophile *S. epidermidis* Y2 at different Mg/Ca molar ratios [100] and different sources of magnesium, XRD analysis of minerals has been performed. Due to no precipitates harvested, the control group was temporarily abandoned. Thus, all the minerals aimed to those in the experimental group. From **Fig. 5**, it can be found that the mineral phases in $MgSO_4$ medium are the same as those in $MgCl_2$ group at each kind of Mg/Ca molar ratio. The mineral phase is calcite at Mg/Ca molar ratio of 0, monohydrocalcite at Mg/Ca molar ratio of 2, 4, 6 and 8. The cell density of monohydrocalcite in $MgCl_2$ group (2.3981) is much lower than that in $MgSO_4$ medium (2.4406), also lower than that in the XRD standard database (2.4105), suggesting that $MgSO_4$ could make monohydrocalcite become much denser. Maybe the changes in density resulted in the crystallinity changes in minerals. There is a significant difference in the crystallinity of minerals between $MgSO_4$ medium and $MgCl_2$ group.

As shown in **Fig. 5,** there are significantly more small peaks in the XRD pattern (**Fig. 5b**) of $MgCl_2$ group than those in $MgSO_4$ group, indicating that the minerals in $MgSO_4$ medium had a higher

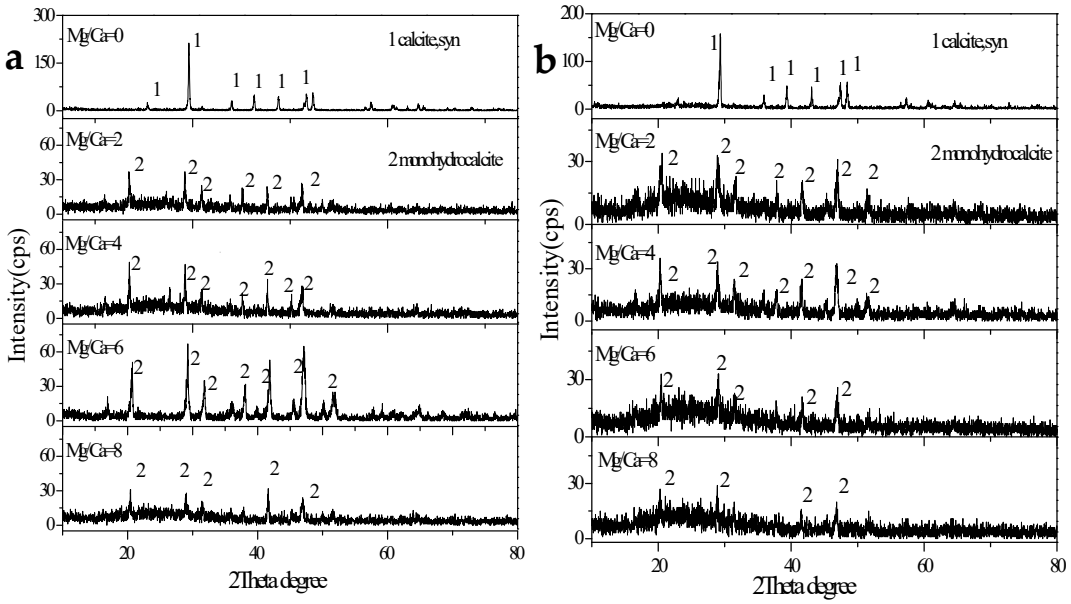

Figure 5. XRD images of minerals in the experimental groups.
(a), the minerals in $MgSO_4$ medium; (b), the minerals in $MgCl_2$ group.

crystallinity than in $MgCl_2$ group. The result revealed that the crystallinity of minerals can be affected differently by different sources of magnesium. Therefore, the crystal cell density and the crystallinity could be affected by different sources of magnesium, and the result showed that the crystal cell density and the crystallinity could become higher in the presence of $MgSO_4$, indicating that the minerals would have a better crystal structure in $MgSO_4$ group than in $MgCl_2$ group.

3.8. SEM and EDS Analyses of Minerals Induced by S. epidermidis Y2 in $MgCl_2$ Group and $MgSO_4$ Group

In order to clearly observe the micromorphology and further determine the elemental composition of minerals, the minerals in different sources of magnesium medium were analyzed by SEM and EDS.

3.8.1. SEM and EDS Analyses of Minerals in $MgSO_4$ Medium

SEM images and EDS analyses of minerals precipitated in $MgSO_4$ medium at different Mg/Ca ratios have been shown in **Fig. 6**. It can be seen from **Fig. 6a1** that the mineral is shaped in dumbbell, approximately 25μm in length, and is growing symmetrically along an axis of symmetry in the middle. The mineral surface is rougher, and some holes in the surface can be observed, which could be considered as a mark left by the shedding of microbial cells from the mineral surface. **Fig. 6a2** shows that the elements of the mineral include C, O, Ca, Al, P, Pt. Pt originated from the spraying operation performed during the sample preparation process. Al derived from the aluminum platform. The presence of P element indicated the involvement of bacteria in the crystal growth process. **Fig. 6b1** shows the fusiform mineral growing symmetrically along the central axis, on which there are not only some holes but some *S. epidermidis* Y2 bacteria. **Fig. 6b2** shows the irregular mineral formed by the interlacing growth of square minerals (**Fig. 6b3**). The mineral shown in **Fig. 6b2** contains C, O, Ca, Al, P and Pt (**Fig. 6b4**). The mineral in **Fig. 6c1** is growing in spiral steps along the central axis, also composed of a large number of square minerals. **Fig. 6c2** shows that the mineral surface is covered by a layer of organic matter, next to the organic matter, there are some *S. epidermidis* Y2 bacteria, on whose surface some nanocrystals with regular geometry

Peer-reviewed version available at Minerals 2018, 8, 594; doi:10.3390/min8120594

appear. Cells with nanocrystals precipitated at the bottom of the medium, which explained why the minerals at the bottom of the medium could contain so many cells. **Fig. 6c3** shows that the mineral shown in **Fig. 6c1** contains C, O, Ca, Al, Na, Cl and P. Na and Cl elements came from the culture medium.

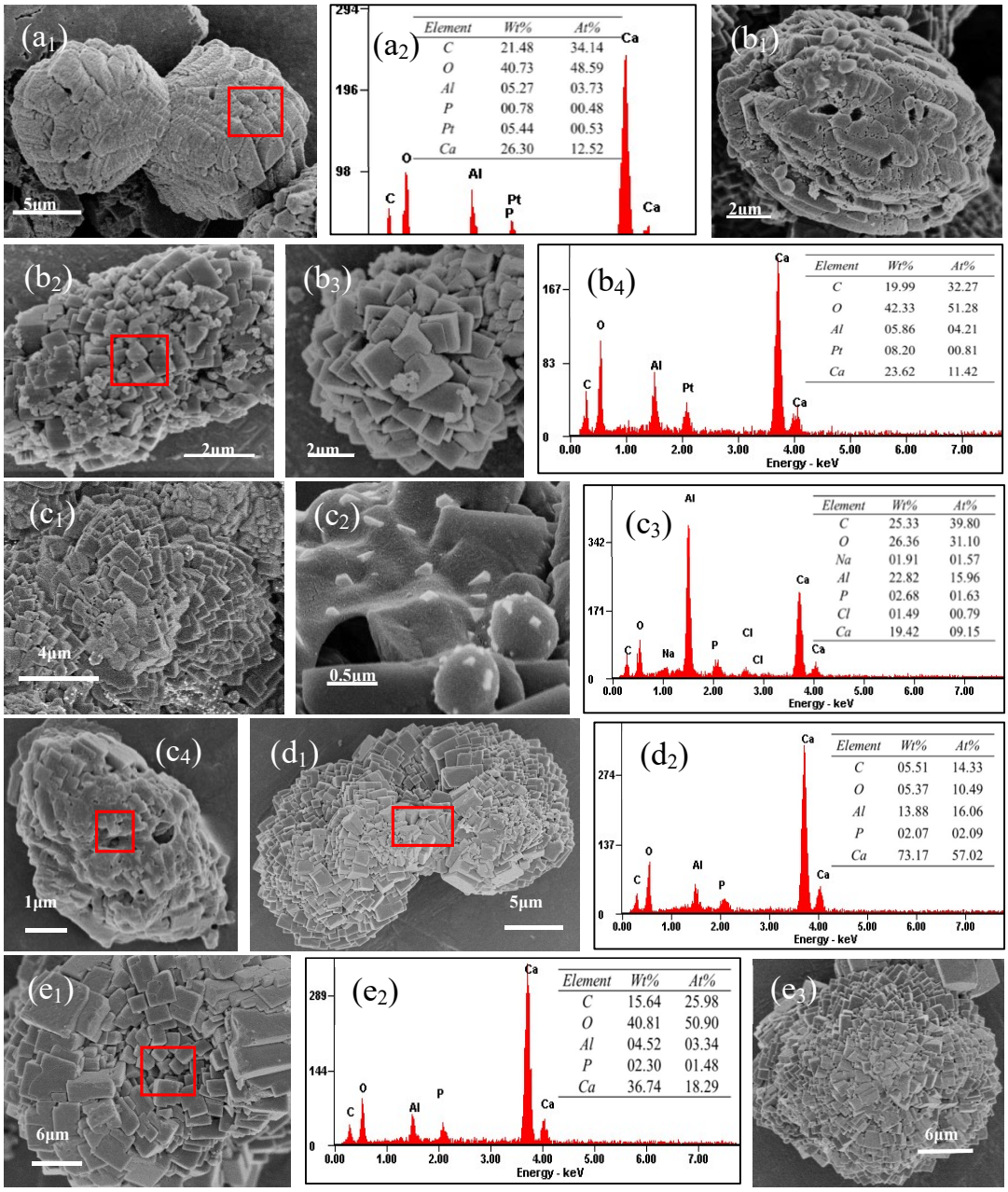

Figure 6. SEM and EDS analyses of minerals in the $MgSO_4$ medium at different Mg/Ca ratios.
(a1)-(a2) Mg/Ca ratio of 0; (b1)-(b4) Mg/Ca ratio of 2; (c1)-(c4) Mg/Ca ratio of 4; (d1)-(d2), Mg/Ca ratio of 6; (e1)-(e3), Mg/Ca ratio of 8.

Fig. 6c4 shows that there is still fusiform mineral at Mg/Ca molar ratio of 4, which was the same as that in **Fig. 6b1**. The rotation step growth pattern of mineral aggregates composed of many minute square minerals is more clearly shown in **Fig. 6d1**. The EDS analysis indicates that the main elements are C, O, Ca, P and Al (**Fig. 6d2**). **Fig. 6e1** reveals that the crystal also grows spirally

Peer-reviewed version available at Minerals 2018, 8, 594; doi:10.3390/min8120594

around the central axis. The main elements are C, O, Ca, P and Al (**Fig. 6e2**). **Fig. 6e3** shows the elliptical mineral that grows in spiral steps along the central axis.

3.8.2. SEM and EDS Analyses of Minerals in $MgCl_2$ Medium

Although the mineral phase is the same as that of $MgSO_4$ medium, there are still significant differences in the micromorphology and growth pattern of minerals. It can be seen from **Figs. 7 a1 and a2** that the mineral is dumbbell-shaped (**Fig. 7a1**) or rodlike (**Fig. 7a2**), covered with many minute rhombohedral crystals. The length of the dumbbell-shaped mineral is about 20 μm and the rodlike mineral is about 15 μm. **Fig. 7a3** shows that the main elements of mineral are C, O, Ca, Al, Na and P. **Figs. 7 b1 and b2** show that the spherical mineral and a unique shaped mineral like a "8" appear, whose surface is covered with small rectangular minerals. The elements in the mineral (**Fig. 7b3**) are the same as those shown in **Fig. 7a3.** There is a significant difference in the crystal growth pattern bwteen $MgSO_4$ group and $MgCl_2$ group. It can be seen from **Fig. 7c1** that the mineral shows a concentric circular growth pattern in $MgCl_2$ group. The inner concentric circular minerals are composed of many small irregular minerals, while the outer concentric circular minerals are closely arranged by many larger long columnar minerals. **Fig. 7c2** shows that the mineral contains C, O, Ca, Mg, Al, Cl and P elements. **Fig. 7c3** shows the micromorphology of the outer concentric circular minerals. It has been found that the minute minerals composed of the concentric circular minerals are long columnar, not square minerals, significantly different from that of $MgSO_4$ group. **Fig. 7d1** shows that the mineral at Mg/Ca molar ratio of 6 is formed by irregular rhombohedral crystals. The minerals have round-cake shape (**Fig. 7d2**) and spherical shape (**Fig. 7d4**). **Fig. 7d3** shows that the mineral contains C, O, Ca, Mg, Al, and P elements. With the increase of Mg^{2+} concentration, the micromorphology of minerals changes significantly. It can be seen from **Figs. 7e1-e3** that the minute minerals covered the surface of dumbell-shaped (**Fig. 7e1**), triangular (**Fig. 7e2**), and irregular minerals (**Fig. 7e3**) become much smaller. The EDS analyses (**Fig. 7e4 and e5**) show many elements are present in the minerals, such as Na, Mg, Al, Cl, and P elements, besides of C, O, Ca elements.

3.9. HRTEM and SAED Analyses of S. epidermidis Y2 Bacterial Superthin Slices

In order to investigate the intracellular biomineralization, superthin slices of *S. epidermidis Y2* bacteria cultured in $MgSO_4$ medium and $MgCl_2$ medium were analyzed by HRTEM and SAED, respectively. **Fig. 8** shows that *S. epidermidis Y2* bacteria are in a shape of grape ball, and have a layered epidermal structure with a lower electron density than inside the cell. The high electron density is related to the thickness of the sample and the metal ions contained. Both in $MgSO_4$ medium and $MgCl_2$ medium, the electron densities in cells are higher, indicating that there were a large number of metal ions inside cells. Due to the characteristics of potassium uptake and sodium rejection by halophilic bacteria in the culture medium rich in NaCl, the higher electron densities maybe revealed the existence of K^+ inside the cell. However, no potassium was present in the culture medium. Therefore, the higher electron densities were maybe due to the presence of Na^+ ions inside the cell. Thus, the superthin slices of *S. epidermidis Y2* bacteria cultivated in culture medium without any Mg^{2+} and Ca^{2+} ions were also investigated, and the result shows that even without Mg^{2+} and Ca^{2+} ions in the culture medium, some regions with higher electron density are still present inside the cells (**Figs. 8f1-f4**). It could be concluded that Na^+ could enter the cell to adjust osmosis, resulting in higher tolerance of *S. epidermidis Y2* bacteria on salt stress because *S. epidermidis Y2* bacteria belong to moderate halophile. At different Mg/Ca molar ratio, higher electron density inside the cell can also be observed in both $MgSO_4$ medium and $MgCl_2$ medium. SAED result shows that there are no diffraction spots and diffraction rings (inset in **Figs. 8c1, c3, e2, e4**), indicating that crystal structure in the higher electron density areas inside the cell was amorphous at Mg/Ca molar ratio of 4 and 8. However, whether Ca and Mg could be contained in these higher electron density areas and whether Mg^{2+} and Ca^{2+} ions could enter the cell is still a question that is needed to further explore. Therefore, the elemental composition of higher electron was also analysed by STEM, which could be found in part 3.10.

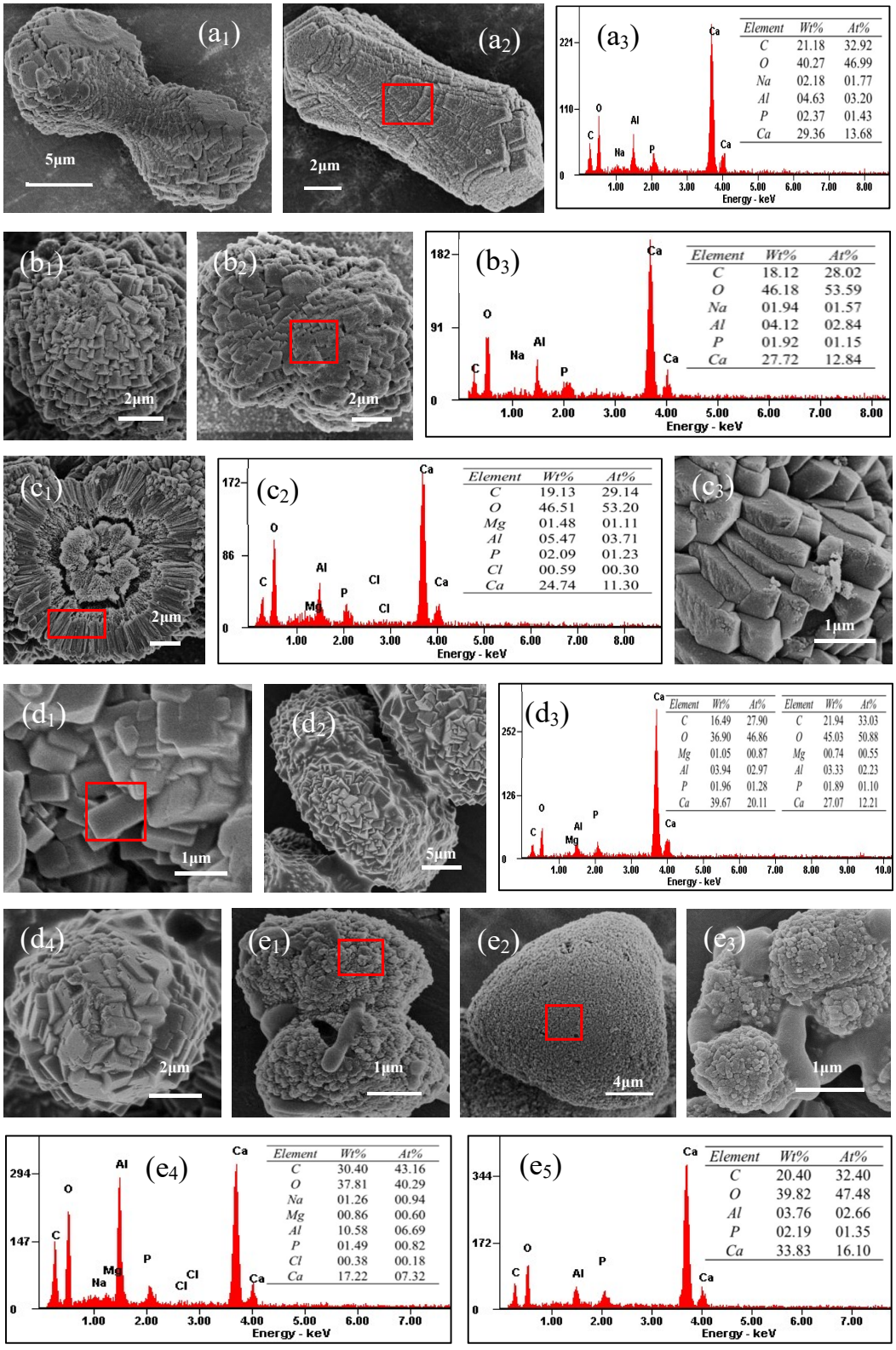

Figure 7. SEM and EDS analyses of minerals in $MgCl_2$ medium at different Mg/Ca ratios.

(a1)-(a3), Mg/Ca ratio of 0; (b1)-(b3), Mg/Ca ratio of 2; (c1)-(c3), Mg/Ca ratio of 4; (d1)-(d4), Mg/Ca ratio of 6; (e1)-(e5), Mg/Ca ratio of 8.

Preprints (www.preprints.org) | NOT PEER-REVIEWED | Posted: 2 November 2018 doi:10.20944/preprints201811.0064.v1

Peer-reviewed version available at Minerals 2018, 8, 594; doi:10.3390/min8120594

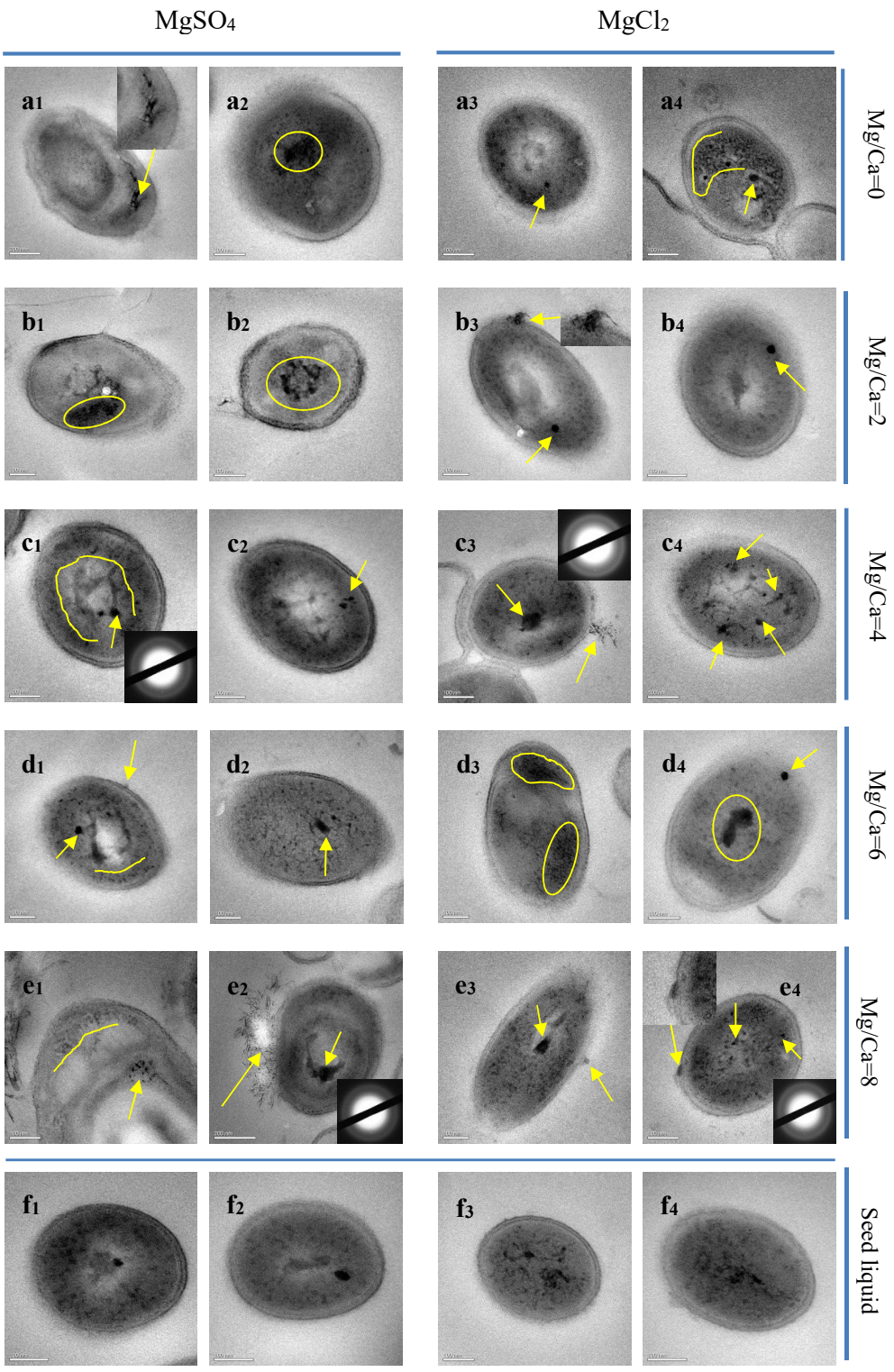

Figure. 8. HRTEM and SAED analyses of *S. epidermidis* Y2 bacterial superthin slices

Among these cells, one that has a crumpled surface is particularly striking, which is shown in **Figs. 9a-c**. The crumpled cells can be found in both $MgSO_4$ medium and $MgCl_2$ medium, which was maybe due to the loss of EPS or aging death. Han et al. [45] have reported that EPS around *Synechocystis sp.* PCC6803 cell can protect the shape of bacteria, and the cells can become crumpled after the EPS is stripped out from the cell under high speed of centrifugation. The number of

Peer-reviewed version available at *Minerals* **2018**, *8*, 594; doi:10.3390/min8120594

crumpled cells in $MgSO_4$ medium is higher than that in $MgCl_2$ medium. **Figs. 9a-c** show that there are also some higher electron density areas inside the crumpled cells, maybe the higher electron density areas were already present inside the cell before they crinkle. **Figs. 9d-f** show that the active cells have a smooth stratified surface without any fold. What's more, the higher electron density area is distributed evenly (**Figs. 9d**) inside the active cells and while only low electron density area distributed unevenly inside the crumpled cells, indicating that the crumpled cells maybe have already begun to degrade.

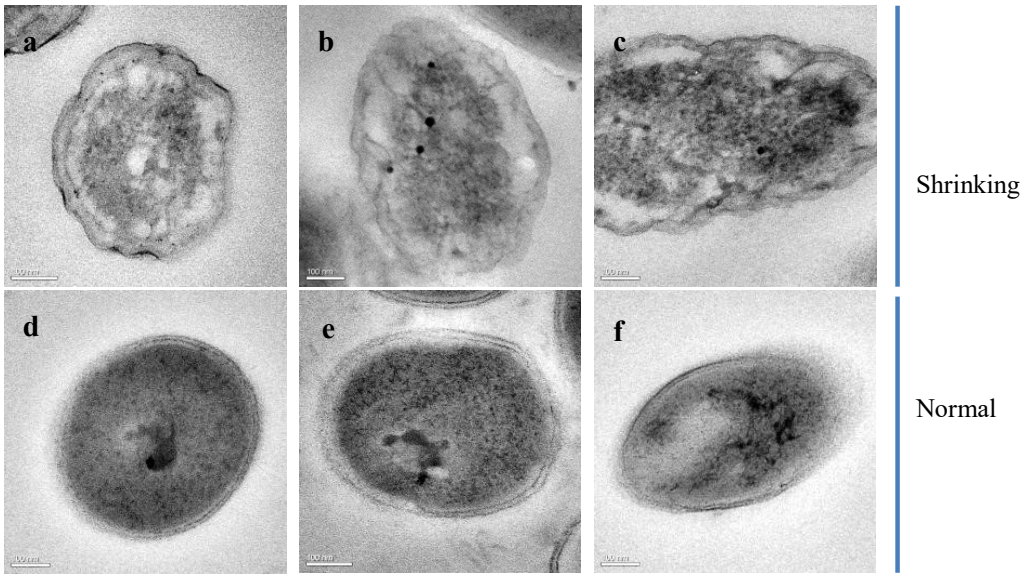

Figure 9. Shinking and normal *S. epidermidis* Y2 cells analyzed by HRTEM.

a-c, Shrinking cells of *S. epidermidis* Y2; d-f, Normal cells of *S. epidermidis* Y2.

3.10 STEM and EDS analyses of the ultrathin slices of S. epidermidis Y2

In order to to further investigate what elements could be contained in these higher electron density areas, STEM-EDS analyses were performed. **Fig. 10** shows that Ca element is present in the higher electron density area at Mg/Ca molar ratio of 0, and both Ca and Mg elements are present at Mg/Ca molar ratio of 4 and 8 in $MgSO_4$ medium and $MgCl_2$ medium. From the distribution of Ca and Mg elements, it can be observed from **Fig. 10** that both calcium and magnesium are more densely distributed inside cells than on the surface, indicating that the organelles or cytoplasm inside the cells were more conducive to adsorbing Ca^{2+} and Mg^{2+} ions, maybe due to the special structure of organelles or the abundant organic matter in the cytoplasm or the liquid condition inside the cell. Therefore, Ca^{2+} and Mg^{2+} ions could enter the cell according to the result of elemental distribution inside the cell. In general, bacteria have protection mechanism to prevent themselves from hurt, e.g. they have cell membrane which is composed of phospholipid bilayers and can prevent soluble micromolecules such as Ca^{2+} and Mg^{2+} ions from entering the cell. How did Ca^{2+} and Mg^{2+} ions enter the cell? There are ions channels of Ca^{2+} and Mg^{2+} embedded the cell membrane, through which these ions can be transferred from the outside to inside the cell by diffusion.

4. Disscusion

4.1. Mechanism of Biomineralization Induced by S. epidermidis Y2 Bacteria

4.1.1. pH Increase

It has been reported by many researchers that the microenvironment around the bacterial cell can be changed by metabolic activities, leading to the microenvironment can reach a supersaturation of some minerals and the precipitation of minerals can be promoted [101]. Among

Peer-reviewed version available at Minerals 2018, 8, 594; doi:10.3390/min8120594

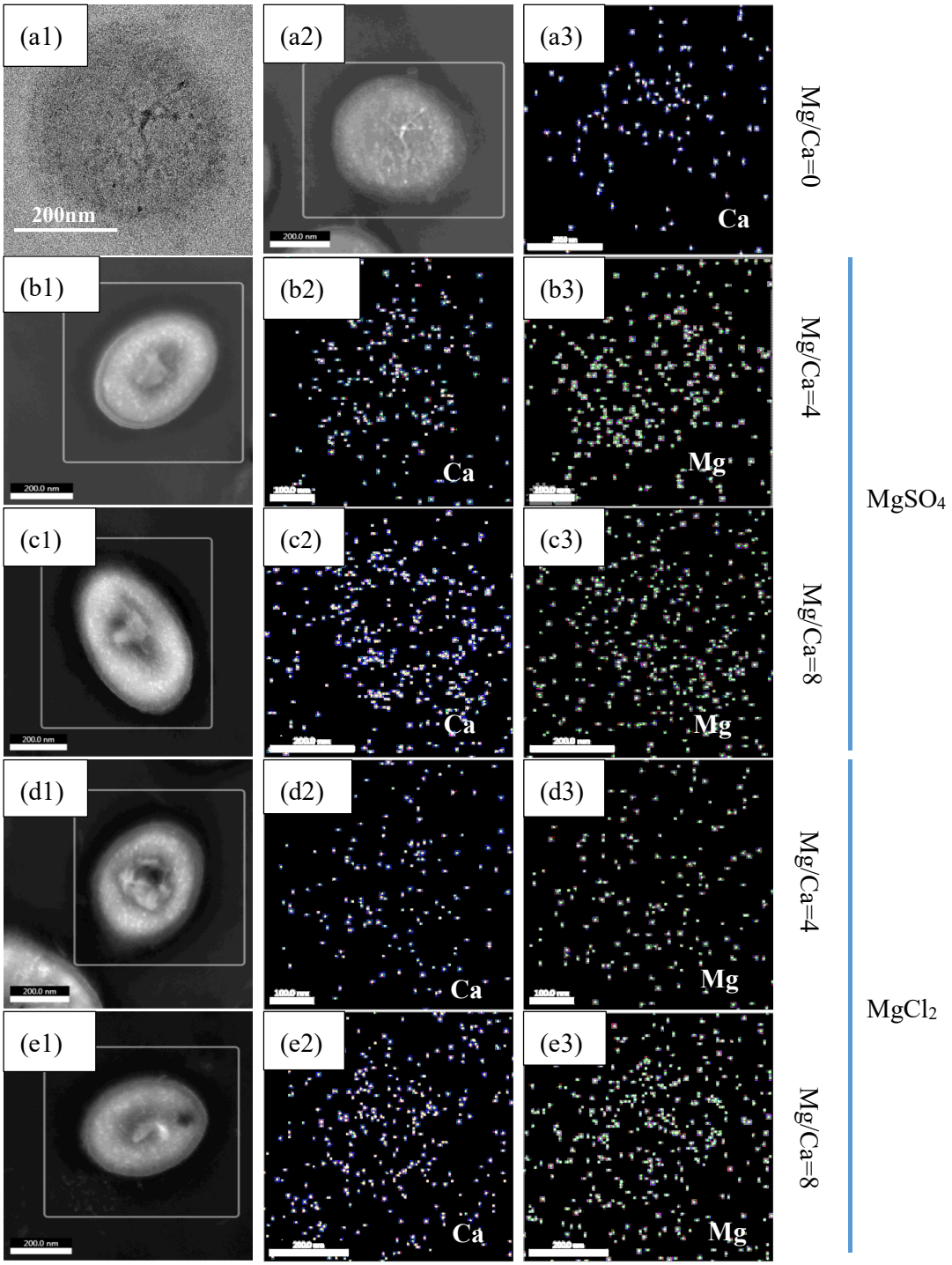

Figure 10. STEM and EDS analyses of the ultrathin slices of *S. epidermidis* Y2.

these changed factors in the environment, pH value is an important factor to influence the biomineralization and has been investigated by many studies [7,25]. Therefore, whether *S. epidermidis* Y2 bacteria could result in pH increase was also tested in this study. The pH of the experimental group inoculated of *S. epidermidis* Y2 bacteria could increase from 7.0 to about 8.7, while the pH in the control group without inoculation of *S. epidermidis* Y2 bacteria remained almost unchanged. The result revealed that the presence of *S. epidermidis* Y2 bacteria could make pH of the liquid culture medium increase. It has confused many researchers about what causes pH to increase so high. Some researchers have investigated the reason of pH increase caused by microorganisms,

Peer-reviewed version available at *Minerals* **2018**, *8*, 594; doi:10.3390/min8120594

and the consensus is that the released ammonia by microorganisms is the main reason [30,60,61]. NH_2- group of amino acids, which are the components of the culture medium, can be transferred from one molecule of amino acid to keto acid by the transamination to form a new amino acid and can also be removed from amino acid to form ammonia by deamination. Ammonia can dissolve into water to release ammonium and hydroxyl ions, thus promoting the pH increase in the culture medium. The equation is as follows:

$$NH_3 + H_2O \rightarrow NH_4^+ + OH^- \quad (1)$$

In this study, ammonia test result was positive, indicating that the released ammonia played an important role in pH increase. In fact, the alkaline environment facilitates the formation of bicarbonate and bicarbonate ions. Microorganisms can increase the utilization efficiency of carbon dioxide through carbon dioxide enrichment mechanism [102]. The carbon dioxide produced by bacterial metabolism and enriched by enrichment mechanism exists in the form of carbonate and bicarbonate ions under alkaline conditions. The equations are as follows (2-4):

$$CO_2 + H_2O \rightarrow H_2CO_3 \quad (2)$$

$$H_2CO_3 + OH^- \rightarrow HCO_3^- + H_2O \quad (3)$$

$$HCO_3^- + OH^- \rightarrow CO_3^{2-} + H_2O \quad (4)$$

Therefore, a large number of OH^-, CO_3^{2-} and HCO_3^- ions can react with Ca^{2+} to form calcium carbonate precipitates when reaching an enough high supersaturation in the liquid culture medium. The equation is as follows (5):

$$OH^- + CO_3^{2-} + HCO_3^- + 2Ca^{2+} \rightarrow 2CaCO_3\downarrow + H_2O \quad (5)$$

4.1.2 CA activity

CA, a kind of metal enzyme, widely exists in animals, plants and prokaryotes, and can catalyze the reversible hydration of carbon dioxide [103]. Carbon dioxide hydrates very slowly in its natural state [104], but the rate increases with the involvement of CA [67,105-108]. In this study, CA can catalyze the hydration reaction of carbon dioxide, coming from the air, bacterial metabolism and carbon dioxide enrichment mechanism, to release carbonate and bicarbonate ions to elevate the supersaturation in the microenvironment around the cell. The equation is as follows (6):

$$CO_2 + H_2O \xrightarrow{CA} H_2CO_3 + OH^- \rightarrow HCO_3^- + CO_3^{2-} \quad (6)$$

From **Fig. 3d**, carbonate ions increases, well consistent with the result shown in equation (6). According to the concentration of carbonate ions, another pH curve could be obtained (**Fig. 3b**). The pH curve based on carbonate ion concentration revealed that due to the presence of carbonate ions, pH values were far beyond those in the experimental group. Therefore, the released carbonate ions by CA catalysis also played an important role in pH increase. Zhuang et al. [62] have also investigated the role of CA played in pH increase, and also believed that CA and ammonia play significant role in pH increase, not only ammonia. In this study, we agree with the opinion. Thus, there were two roles played by CA: one was to increase pH, and the other was to catalyze the hydration of carbon dioxide to produce carbonate ions and bicarbonate ions. Due to the high efficiency of enzyme catalysis, CA can quickly catalyze hydration of carbon dioxide to release bicarbonate and carbonate ions, and then promote the precipitation of carbonate minerals. In this process, CA plays an important role. Liu et al. [109] have reported that CA can be used to accelerate an aqueous processing route to carbonate formation. Sundaram et al. [110] have proved that calcite formation is successfully obtained by using *Bacillus* sp. with enhanced activity of CA, a much higher rate of $CaCO_3$ precipitation can be observed with increased CA activity. Similar reports have been documented by Mirjafari et al. [111], Srivastava et al. [112] and Ramanan et al. [113].

Peer-reviewed version available at Minerals 2018, 8, 594; doi:10.3390/min8120594

4.2. The Role of Mg^{2+} Ions on Monohydrocalcite

In this study, calcite was the mineral produced when the ratio of magnesium to calcium was zero, and monohydrocalcite at other Mg/Ca molar ratios. Studies have shown that magnesium ions play an important role in the formation of monohydrocalcite [114]. According to XRD analysis, monohydrocalcite appeared in both $MgSO_4$ medium and $MgCl_2$ medium. With increased Mg/Ca ratio, the mineral phase did not change.

By comparision with calcite and aragonite, monohydrocalcite is thermodynamically unstable under the temperature and pressure of the earth's surface, which determines the low abundance of this mineral phase [114]. Howerver, monohydrocalcite can be found in a variety of natural environments, such as saline spring [115], caves [116], and deep sediments in lake [117]. Besides this, monohydrocalcite is also a product of biomineralization, which can be formed by some molluscs [118], flatworms [119], vertebrates [120], guinea pigs [121], Saguaro cacti [122,123], algae [124] and halo bacilli [125]. Although the distribution of monohydrocalcite is relatively extensive, its formation mechanism is still not very clear.

Many researchers have reported that Mg is almost present in all natural and synthetic monohydrocalcite crystals [124,126]. The Mg content of the liquid culture medium, which was used to form monohydrocalcite, played a significant role in its formation. It has been reported that a higher Mg/Ca molar ratio in the precipitating solution is a prerequisite for the formation of both natural and biogenic monohydrocalcites [127]. In aqueous solutions without magnesium ions, monohydrocalcite is converted to calcite [128,129]. Some researchers have suggested that the growth rate of calcite is closely related to Mg^{2+} ions, always inversely proportional to the Mg concentration [130]. The existence of magnesium ions can inhibit the formation of calcite and keep monohydrocalcite stable. The inhibition of Mg on other Ca–Mg carbonates has also been reported [131]. The crystallinity and particle size of formed monohydrocalcite can decrease with Mg content, which also shows that Mg is a key component in monohydrocalcite [126].

In this study, calcium ions could easily combine with carbonate ions to form calcium carbonate, while Mg-carbonate minerals could not be obtained even though the Mg^{2+} ion concentration was 8-fold Ca^{2+} ion concentration. The reason has been explored by many researchers. Now, one of the opinions that's generally accepted is that the stronger hydration shell of Mg with respect to Ca results in Mg-carbonate minerals are difficult to form [132]. The energy used to dehydrate before Mg incorporating into a carbonate crystal is much higher than that of Ca [55,57], which controls the kinetics of crystal growth [133]. Therefore, monohydrocalcite growth would be favored in this study.

4.3. Effects of Different Mg^{2+} on Monohydrocalcite Crystal

During the mineralization process induced by *S. epidermis*, different Mg^{2+} could control the crystal structure and growth mode of the mineral particles. The crystal structure and growth mode of minerals in $MgSO_4$ medium are significantly different from those in $MgCl_2$ medium. In this study, the crystal density of monohydrocalcite in $MgSO_4$ medium was higher than that in $MgCl_2$ medium, indicating that different sources of Mg^{2+} could affect the crystal structure and make the cell structure more compact. Besides the hydration membrane covered the surface of Mg^{2+} ions, SO_4^{2-} ions could also adsorb Mg^{2+} to form ion pairs in the liquid culture medium, thus, maybe due to the reason, the reaction of Mg^{2+} ion displacing Ca^{2+} ion was inhibited and the effect of Mg^{2+} on monohydrocalcite in $MgSO_4$ medium was little. XRD analysis also shows the crystallinity of monohydrocalcite in $MgSO_4$ medium is also higher than that in $MgCl_2$ medium, which further revealed that Mg^{2+} ions were easier to enter monohydrocalcite crystal and could affect the crystal cell structure more intensely in $MgCl_2$ medium. Fukushi et al. [134] have reported the detailed mechanism of monohydrocalcite crystal structure becoming looser due to the displacement by Mg^{2+} ions in $MgCl_2$ solution. In the structure of monohydrocalcite, Ca atoms are surrounded by two H_2O molecules and four CO_3^{2-}, that is to say, surrounded by eight oxygen atoms, including one oxygen atom from two CO_3^{2-}, two oxygen atoms from two CO_3^{2-} and one oxygen atom from two H_2O

molecules (**Fig. 11a**). If Ca was replaced by Mg atom in the structure of monohydrocalcite, the arrangement of CO_3^{2-} and H_2O molecules around Mg^{2+} would be changed. After the replacement, the crystal structure was changed from the CaO_8 polyhedra (**Fig. 11a**) to the MgO_6 polyhedra (**Fig. 11b**), due to the fact that the rotation and movement occurred to the two CO_3^{2-} groups, which provided two oxygen atoms to CaO_8 polyhedra [134]. In the MgO_6 octahedron, the Mg-O bond lengths (between Mg and O of CO_3) are 2.058–2.186 A°, and 2.296–2.411 A° (between Mg and O of H_2O), significantly smaller than that of Ca-O [134]. In this case, the unit cell of monohydrocalcite was slightly deformed.

The growth mode of crystals also revealed the significant role played by different sources of Mg^{2+}. In $MgSO_4$ solution, the mineral grew in a spiral staircase pattern, while in $MgCl_2$ solution the mineral grew in a concentric circular pattern. The theory of the classical crystallization proposed by Bettina et al. [135] maybe could be applied to the growth mode in this study, and the change of free energy maybe was the main reason for the crystal spiral growth mode. Growth rates can also influence the mineral morphology [136,137]. In this study, the mineral with a shape of concentric circular ring shown in **Fig. 7c1** was formed maybe due to the different growth rate in $MgCl_2$ solution. The inner mineral grew at a quicker rate than the outer mineral, therefore, the inner

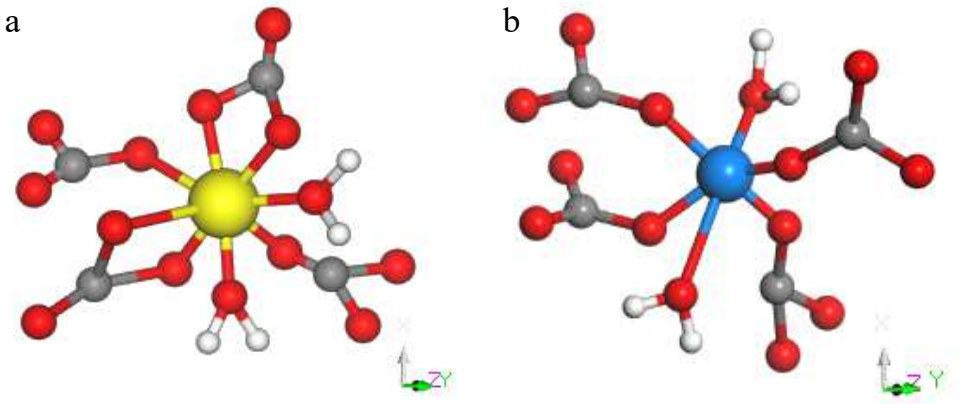

Figure 11. Local arrangements of monohydrocalcite provided by Fukushi et al. (2017). a, the standard crystal structure of monohydrocalcite, CaO_8 polyhedron; b, the changed crystal structure after replacement by Mg atom, MgO_6 polyhedron. The red sphere represents O, gray spheres denote C, white denotes H from H_2O, yellow denotes Ca, and blue denotes Mg.

mineral was composed of a large number of minute crystals without regular shape and the outer mineral was aggregated by larger crystals with rhombohedral shape. EPS composition analysis showed that there were a large number of amino acids. Under alkaline conditions, the cell surface had a large number of negative charges. Therefore, the concentration of Ca^{2+} ions may be higher on the periphery of the cell aggregation, while lower away from the cells. The concentration grade of Ca^{2+} ions may lead to different growth rates of mineral crystals, leading to the formation of concentric circular minerals. There are only few studies on the growth mode of minerals obtained from different sources of magnesium, and further studies are needed.

5. Conclusions

Different sources of magnesium significantly affected the crystal cell structure in the process of carbonate biomineralization induced by *S. epidermidis* Y2 bacteria. *S. epidermidis* Y2 bacteria could produce the ammonia and CA to increase pH and to elevate the supersaturation of minerals, thus promoting the precipitation of carbonates. The crystal cell density of monohydrocalcite was lower in $MgCl_2$ medium than that in $MgSO_4$ medium. The crystal grew in a mode of spiral staircas in $MgSO_4$ medium, while grew in a concentric circular pattern in $MgCl_2$ medium. This study may be helpful to further understand the biomineralization mechanism, may also provide some references for the reconstruction of paleogeological environment.

Acknowledgments: This work was supported by the National Natural Science Foundation of China (41772095, U1663201, 41702131), Taishan Scholar Talent Team Support Plan for Advanced & Unique Discipline Areas, Major Scientific and Technological Innovation Projects of Shandong Province (2017CXGC1602, 2017CXGC1603), SDUST Research Fund (2015TDJH101), Natural Science Foundation of Shandong Province (ZR2017BD001), the China Postdoctoral Science Foundation founded project (2016M600548, 2017T100502), Qingdao Postdoctoral Applied Research Project (2015199), the Scientific and Technological Innovation Project Financially Supported by Qingdao National Laboratory for Marine Science and Technology (No. 2016ASKJ13), Open Fund of the Key Laboratory of Marine Geology and Environment, Chinese Academy of Sciences (No. MGE2016KG10), Postgraduate Science and Technology Innovation Project of Shandong University of Science and Technology (SDKDYC180105, SDKDYC180211).

Author Contributions: Zuozhen Han and Huaxiao Yan conceived and designed the experiments; Wenwen Yu performed the experiments; Zuozhen Han and Huaxiao Yan analyzed the results of all the experiments; Yanhong Zhao was in charge of calculation; Wenwen Yu and Huaxiao Yan wrote the paper. Huaxiao Yan and Maurice E. Tucker revised the manuscript. All authors read and approved the manuscript.

References

1. Bakhshi, E.; Torab, F.M. Determining Wettability of Fractured Carbonate Reservoirs. *Natural Resources Research* **2016**, *25*, 211-225, DOI: 10.1007/s11053-015-9282-z.
2. Correia, M.G.; Maschio, C.; Schiozer, D.J. Integration of multiscale carbonate reservoir heterogeneities in reservoir simulation. *J. Petrol. Sci. Eng.* **2015**, *131*, 34-50, DOI: 10.1016/j.petrol.2015.04.018.
3. Chang, X.C.; Shi, B.B.; Han, Z.Z.; Li, T.T. C_5-C_{13} light hydrocarbons of crude oils from northern Halahatang oilfield (Tarim Basin, NW China) characterized by comprehensive two-dimensional gas chromatography. *J. Petrol. Sci. Eng.* **2017**, *157*, 223-231, DOI: 10.1016/j.petrol.2017.07.043.
4. Van Loon, A.J.; Han, Z.Z.; Han, Y. Origin of the vertically orientated clasts in brecciated shallow-marine limestones of the Chaomidian Formation (Furongian, Shandong Province, China). *Sedimentology* **2013**, *60*, 1059-1070, DOI: 10.1111/sed.12018.
5. Chen, J.T.; Van Loon, A.; Han, Z.Z.; Chough, S.K. Funnel-shaped, breccia-filled clastic dykes in the Late Cambrian Chaomidian Formation (Shandong Province, China). *Sediment. Geol.* **2009**, *221*, 1-6, DOI: 10.1016/j.sedgeo.2009.09.006.
6. Yang, R.C.; Fan, A.P.; Han, Z.Z.; Chi, N.J.; Yu, H. Characteristics and genesis of microbial lumps in the Maozhuang Stage (Cambrian Series 2), Shandong Province, China. *Sci. China. Earth. Sci.* **2013**, *56*, 494-503, DOI: 10.1007/s11430-012-4539-4.
7. Han, Z.Z.; Meng, R.R.; Yan, H.X.; Zhao, H.; Han, M.; Zhao, Y.Y.; Sun, B.; Sun, Y.B.; Wang, J.; Zhuang, D.X. Calcium carbonate precipitation by Synechocystis sp. PCC6803 at different Mg/Ca molar ratios under the laboratory condition. *Carbonate. Evaporite.* **2016**, *32*, 561-575, DOI: 10.1007/s13146-016-0322-5.
8. Chen, J.T.; Chough, S.K.; Han, Z.Z.; Lee, J.H. An extensive erosion surface of a strongly deformed limestone bed in the Gushan and Chaomidian formations (late Middle Cambrian to Furongian), Shandong Province, China: Sequence–stratigraphic implications. *Sediment. Geol.* **2011**, *233*, 129-149, DOI: 10.1016/j.sedgeo.2010.11.002.
9. Lee, J.H.; Chen, J.T.; Chough, S.K. Paleoenvironmental implications of an extensive maceriate microbialite bed in the Furongian Chaomidian Formation, Shandong Province, China. *Palaeogeogr. Palaeocl.* **2010**, *297*, 621-632, DOI: 10.1016/j.palaeo.2010.09.012.
10. Bose, S.; Chakrabarti, G.; Shome, D. Evolution of Palaeo-Mesoproterozoic open coast ramp-clues from stromatolite-bearing carbonate facies of Vempalle Formation, Cuddapah Basin, India. *Arab. J. Geosci.* **2017**, *10*, DOI: 10.1007/s12517-017-2988-y.
11. Siahi, M.; Hofmann, A.; Hegner, E.; Master, S. Sedimentology and facies analysis of Mesoarchaean stromatolitic carbonate rocks of the Pongola Supergroup, South Africa. *Precambrian. Res.* **2016**, *10*, 244-264, DOI: 10.1007/s12517-017-2988-y.

12. Spadafora, A.; Perri, E.; Mckenzie, J.A.; Vasconcelos, C. Microbial biomineralization processes forming modern Ca:Mg carbonate stromatolites. *Sedimentology* **2010**, *57*, 27-40, DOI: 10.1111/j.1365-3091.2009.01083.x.
13. Han, Z.Z.; Chen, J.T.; Chi, N.J.; Wang, Z.P.; Yang, R.C.; Fan, A.P. Microbial carbonates: a review and perspectives. *Marine Geology & Quaternary Geology* **2009**, *29*, 29-38, DOI: 10.3724/SP.J.1140.2009.04029.
14. Chough, S.K.; Lee, H.S.; Woo, J.; Chen, J.T.; Choi, D.K.; Lee, S.B.; Kang, I.; Park, T.Y.; Han, Z.Z. Cambrian stratigraphy of the North China Platform: revisiting principal sections in Shandong Province, China. *Geosci. J.* **2010**, *14*, 235-268. DOI: 10.1007/s12303-010-0029-x.
15. Bull, A.T. Microbial diversity and bioprospecting. *Microbial Diversity & Bioprospecting* **2004**.
16. Banfield, J.F.; Cervini-Silva, J.; Nealson, K.H. *Molecular geomicrobiology*; Mineralogical Society of America: 2005.
17. Castello, J.; Rogers; Scott. Life in Ancient Ice. *Princeton University Press* **2005**.
18. Balkwill, D.L. Geomicrobial Processes and Biodiversity in the Deep Terrestrial Subsurface. *Geomicrobiol. J.* **2006**, *23*, 345-356, DOI: 10.1080/01490450600875571.
19. Dong, H.L. Mineral-microbe interactions: a review. *Frontiers of Earth Science in China* **2010**, *4*, 127-147, DOI: 10.1007/s11707-010-0022-8.
20. Cassarino, G.; Olzi, E.; Rizzo, R. Bacterially induced mineralization of calcium carbonate in terrestrial environments: The role of exopolysaccharides and amino acids. *J. Sediment. Res.* **2003**, *73*, 485-490, DOI: 10.1306/111302730485.
21. Yoshimura, T.; Tamenori, Y.; Suzuki, A.; Kawahata, H.; Iwasaki, N.; Hasegawa, H.; Luan, T.N.; Kuroyanagi, A.; Yamazaki, T.; Kuroda, J. Altervalent substitution of sodium for calcium in biogenic calcite and aragonite. *Geochim. Cosmochim. Ac.* **2016**, *202*.
22. Menadakis, M.; Maroulis, G.; Koutsoukos, P.G. Incorporation of Mg^{2+} , Sr^{2+} , Ba^{2+} and Zn^{2+} into aragonite and comparison with calcite. *J. Math. Chem.* **2009**, *46*, 484-491, DOI: 10.1007/s10910-008-9490-4.
23. Weiner; Stephen. *On biomineralization*; Oxford University Press: 1989; pp. 119-130.
24. Dittrich, M.; Müller, B.; Mavrocordatos, D.; Wehrli, B. Induced Calcite Precipitation by Cyanobacterium Synechococcus. *CLEAN - Soil, Air, Water*. **2003**, *31*, 162-169, DOI: 10.1002/aheh.200300486.
25. Thompson, J.B.; Ferris, F.G. Cyanobacterial precipitation of gypsum, calcite, and magnesite from natural alkaline lake water. *Geology* **1990**, *18*, 995.
26. Han, Z.Z.; Zhuang, D.X.; Yan, H.X.; Zhao, H.; Sun, B.; Li, D.; Sun, Y.W.; Hu, W.Y.; Xuan, Q.Z.; Chen, J.A. Thermogravimetric and kinetic analysis of thermal decomposition characteristics of microbial calcites induced by cyanobacteria *Synechocystis sp*. PCC6803. *J. Therm. Anal. Calorim.* **2017**, *2017*, 1-9, DOI: 10.1007/s10973-016-6026-1.
27. Benzerara, K.; Skouripanet, F.; Li, J.; Férard, C.; Gugger, M.; Laurent, T.; Couradeau, E.; Ragon, M.; Cosmidis, J.; Menguy, N. Intracellular Ca-carbonate biomineralization is widespread in cyanobacteria. *P. Natl. Acad. Sci. USA.* **2014**, *111*, 10933-10938, DOI: 10.2307/23804968.
28. Stocks-Fischer, S.; Galinat, J.K.; Bang, S.S. Microbiological precipitation of $CaCO_3$. *Soi.l Biol. Biochem.* **1999**, *31*, 1563-1571, DOI: 10.1016/S0038-0717(99)00082-6.
29. Han, Z.Z.; Li, D.;Zhao, H.; Yan, H.X.; Li, P.Y. Biomineralization of Carbonate Minerals Induced by the Halophilic Chromohalobacter israelensis under High Salt Concentrations: Implications for Natural Environments. *Minerals* **2017**, *7*, DOI: 10.3390/min7060095.
30. Sánchez-Román, M.; Rivadeneyra, M.A.; Vasconcelos, C.; McKenzie, J.A. Biomineralization of carbonate and phosphate by moderately halophilic bacteria. *Fem.s Microbiol. Ecol.* **2007**, *61*, 273-284, DOI: 10.1111/j.1574-6941.2007.00336.x.
31. Ma, R.F.; Quevedo-Sarmiento, J.; Rivadeneyra, M.A.; Bejar, V.; Delgado, R.; Ramos-Cormenzana, A. Calcium carbonate precipitation by two groups of moderately halophilic microorganisms at different temperatures and salt concentrations. *Curr. Microbiol.* **1988**, *17*, 221-227, DOI: 10.1007/BF01589456.
32. Almahamedh, H.H. NACE International Store - Sulfate Reducing Bacteria Influenced Calcium Carbonate Precipitation. **2013**.
33. Zhang, F.F.; Xu, H.F.; Shelobolina, E.S.; Converse, B.; Converse, B.; Shen, Z.Z.; Roden, E.E. The catalytic effect of bound extracellular polymeric substances excreted by anaerobic microorganisms on Ca-Mg carbonate precipitation: Implications for the "dolomite problem". *Am. Mineral.* **2015**, *100*, 483-494, DOI: 10.2138/am-2015-4999.

34. Han, Z.Z.; Zhao, Y.Y.; Yan, H.X.; Zhao, H.; Han, M.; Sun, B.; Sun, X.Y.; Hou, F.F.; Sun, H.; Han, L. Struvite Precipitation Induced by a Novel Sulfate-Reducing Bacterium Acinetobacter calcoaceticus SRB4 Isolated from River Sediment. *Geomicrobiol. J.* **2015**, *32*, 868-877, DOI: 10.1080/01490451.2015.1016247.
35. Kenward, P.A.; Goldstein, R.H.; González, L.A.; Roberts, J.A. Precipitation of low-temperature dolomite from an anaerobic microbial consortium: the role of methanogenic Archaea. *Geobiology* **2009**, *7*, 556-565, DOI: 10.1111/j.1472-4669.2009.00210.x.
36. Barnes, R.; Goldberg, E. Methane production and consumption in anoxic marine sediments. *Geology* **1976**, *4*, 297-300.
37. Deppenmeier, U. The unique biochemistry of methanogenesis. *Prog. Nucleic. Acid. Re.* **2002**, *71*, 223-283, DOI: 10.1016/S0079-6603(02)71045-3.
38. Zehnder, A.J.; Brock, T.D. Methane formation and methane oxidation by methanogenic bacteria. *J. Bacteriol.* **1979**, *137*, 420-432.
39. Douglas, S.; Yang, H.X. Mineral biosignatures in evaporites: Presence of rosickyite in an endoevaporitic microbial community from Death Valley, California. *Geology* **2002**, *30*, 1075-1078, DOI: 10.1130/0091-7613(2002)030<1075:MBIEPO>2.0.CO;2.
40. Knauth, L.P. Salinity history of the Earth's early ocean [letter]. *Nature* **1998**, *395*, 554-555, DOI: 10.1038/26879.
41. Chen, J.T.; Chough, S.K.; Lee, J.H.; Han, Z.Z. Sequence-stratigraphic comparison of the upper Cambrian Series 3 to Furongian succession between the Shandong region, China and the Taebaek area, Korea: high variability of bounding surfaces in an epeiric platform. *Geosci. J.* **2012**, *16*, 357-379, DOI: 10.1007/s12303-012-0040-5.
42. Han, Z.Z.; Zhang, X.L.; Chi, N.J.; Han, M.; Woo, J.; Lee, H.S.; Chen, J.T. Cambrian oncoids and other microbial-related grains on the North China Platform. *Carbonate. Evaporite.* **2015**, *30*, 373-386, DOI: 10.1007/s13146-014-0209-2.
43. Zhang, X.G.; Lin, C.Y.; Zahid, M.A.; Jia, X.P.; Zhang, T. Paleosalinity and water body type of Eocene Pinghu Formation, Xihu Depression, East China Sea Basin. *J. Petrol. Sci. Eng.* **2017**, *158*, DOI: 10.1016/j.petrol.2017.08.074.
44. Han, Z.Z.; Yan, H.X.; Zhou, S.X.; Zhao, H.; Zhang, Y.; Zhang, N.N.; Yao, C.K.; Zhao, L.; Han, C.Y. Precipitation of calcite induced by *Synechocystis sp*. PCC6803. *World. J. Microb. Biot.* **2013**, *29*, 1801-1811, DOI: 10.1007/s11274-013-1341-1
45. Han, Z.Z.; Yan, H.X.; Zhao, H.; Zhou, S.X.; Han, M.; Meng, X.Q. Bio-precipitation of Calcite with Preferential Orientation Induced by *sp*. PCC6803. *Geomicrobiol. J.* **2014**, *31*, 884-899, DOI: 10.1080/01490451.2014.907379.
46. Han, Z.Z.; Zhao, Y.Y.; Yan, H.X.; Zhao, H.; Han, M.; Sun, B.; Meng, R.R.; Zhuang, D.X.; Li, D.; Gao, W.J. The Characterization of Intracellular and Extracellular Biomineralization Induced by Synechocystis sp. PCC6803 Cultured under Low Mg/Ca Ratios Conditions. *Geomicrobiol. J.* **2016**, *34*, 362-373, DOI: 10.1080/01490451.2016.1197986.
47. Yan, H., Xiao; Han, Z.Z.; Zhao, H.; Zhou, S.X.; Chi, N.J.; Han, M.; Kou, X.Y. Characterization of calcium deposition induced by *Synechocystis sp.* PCC6803 in BG11 culture medium. *Chin. J. Oceanol. Limn.* **2014**, *32*, 503-510, DOI: 10.1007/s00343-014-3150-2.
48. Sobolev, N.V.; Schertl, H.P.; Neuser, R.D.; Tomilenko, A.A.; Kuzmin, D.V.; Logvinova, A.M.; Tolstov, A.V.; Kostrovitsky, S.I.; Yakovlev, D.A.; Oleinikov, O.B. Formation and evolution of hypabyssal kimberlites from the Siberian craton: Part 1 – New insights from cathodoluminescence of the carbonates. *J. Asian. Earth. Sci.* **2017**, *145*, 670-678, DOI: 10.1016/j.jseaes.2017.06.009.
49. Rivadeneyra, M.A.; Delgado, G.; Soriano, M.; Ramos-Cormenzana, A.; Delgado, R. Precipitation of carbonates by Nesterenkonia halobia in liquid media. *Chemosphere* **2000**, *41*, 617-624, DOI: 10.1016/S0045-6535(99)00496-8.
50. Rivadeneyra, M.A.; Delgado, R.; Moral, A.D.; Ferrer, M.R.; Ramos-Cormenzana, A. Precipatation of calcium carbonate by Vibrio spp. from an inland saltern. *Fems. Microbiol. Ecol.* **1994**, *13*, 197-204, DOI: 10.1111/j.1574-6941.1994.tb00066.x.
51. Parraga, J.; Rivadeneyra, M.A.; Delgado, R.; Iniguez, J.; Soriano, M.; Delgado, G. Study of biomineral formation by bacteria from soil solution equilibria. *React. Funct. Polym.* **1998**, *36*, 265–271, DOI: 10.1016/S1381-5148(97)00158-2.

52. Ferrer, M.R.; Quevedo-Sarmiento, J.; Bejar, V.; Delgado, R.; Ramos-Cormenzana, A.; Rivadeneyra, M.A. Calcium carbonate formation by Deleya halophila: Effect of salt concentration and incubation temperature. *Geomicrobiol. J.* **1988**, *6*, 49-57, DOI: 10.1080/01490458809377821.
53. Buczynski, C.; Chafetz, H.S. Habit of bacterially induced precipitates of calcium carbonate and the influence of medium viscosity on mineralogy. *J. Sediment. Res.* **1991**, *61*, 226-233.
54. Kropp, J.; Block, A.; Bloh, W.V.; Klenke, T.; Schellnhuber, H.J. Multifractal characterization of microbially induced magnesian calcite formation in Recent tidal flat sediments. *Sediment. Geol.* **1997**, *109*, 37-52, DOI: 10.1016/S0037-0738(96)00059-0.
55. Qiu, X.; Wang, H.M.; Yao, Y.C.; Duan, Y. High salinity facilitates dolomite precipitation mediated by Haloferax volcanii DS52. *Earth. Planet. Sc. Lett.* **2017**, *472*, 197-205, DOI: 10.1016/j.epsl.2017.05.018.
56. Qiu, X.; Yao, Y.C.; Wang, H.M.; Duan, Y. Live microbial cells adsorb Mg^{2+} more effectively than lifeless organic matter. *Front. Earth. Sci-Prc.* **2018**, *12*, 160-169, DOI: 10.1007/s11707-017-0626-3.
57. Deng, S.C.; Dong, H.L.; Lv, G.; Jiang, H.C.; Yu, B.S.; Bishop, M.E. Microbial dolomite precipitation using sulfate reducing and halophilic bacteria: Results from Qinghai Lake, Tibetan Plateau, NW China. *Chem. Geol.* **2010**, *278*, 151-159, DOI: 10.1016/j.chemgeo.2010.09.008.
58. Bundeleva, I.A.; Shirokova, L.S.; Bénézeth, P.; Pokrovsky, O.S.; Kompantseva, E.I.; Balor, S. Calcium carbonate precipitation by anoxygenic phototrophic bacteria. *Chem. Geol.* **2012**, *291*, 116-131, DOI: 10.1016/j.chemgeo.2011.10.003.
59. Rivadeneyra, M.A.; Delgado, R.; Párraga, J.; Ramos-Cormenza, A.; Delgado, G. Precipitation of minerals by 22 species of moderately halophilic bacteria in artificial marine salts media: influence of salt concentration. *Folia Microbiol.* **2006**, *51*, 445-453, DOI: 10.1007/BF02931589.
60. Grasby, S. Naturally precipitating vaterite (μ-$CaCO_3$) spheres: unusual carbonates formed in an extreme environment. *Geochim. Cosmochim. Ac.* **2003**, *67*, 1659-1666.
61. Wei, S.P.; Cui, H.P.; Jiang, Z.L.; Liu, H.; He, H.; Fang, N.Q. Biomineralization processes of calcite induced by bacteria isolated from marine sediments. *Brazilian Journal of Microbiology* **2015**, *46*, 455–464, DOI: 10.1590/S1517-838246220140533.
62. Zhuang, D.X.; Yan, H.X.; Tucker, M.E.; Zhao, H.; Han, Z.Z.; Zhao, Y.H.; Sun, B.; Li, D.; Pan, J.T.; Zhao, Y.Y.; Meng, R.R.; Shan, G.H.; Zhang, X.K.; Tang, R.Z. Calcite precipitation induced by Bacillus cereus MRR2 cultured at different Ca^{2+} concentrations: Further insights into biotic and abiotic calcite. *Chem. Geol.* **2018**, DOI: 10.1016/j.chemgeo.2018.09.018.
63. Han, Z.Z.; Zhao, Y.Y.; Yan, H.X.; Zhao, H.; Han, M.; Sun, B.; Meng, R.R.; Zhuang, D.X.; Li, D.; Gao, W.J. The Characterization of Intracellular and Extracellular Biomineralization Induced by Synechocystis sp. PCC6803 Cultured under Low Mg/Ca Ratios Conditions. *Geomicrobiol. J.* **2017**, *34*, 362-373, DOI: 10.1080/01490451.2016.1197986.
64. Thatcher, B.; Doherty, A.; Orvisky, E.; Martin, B.; Henkin, R. Gustin from human parotid saliva is carbonic anhydrase VI. *Biochem. Bioph. Res. Co.* **1998**, *250*, 635-641, DOI: 10.1006/bbrc.1998.9356.
65. Lindskog, S. Structure and mechanism of carbonic anhydrase. *Pharmacol Ther* **1997**, *74*, 1-20.
66. Li, W.; Liu, L.P.; Chen, W.S.; Yu, L.J.; Li, W.B.; Yu, H.Z. Calcium carbonate precipitation and crystal morphology induced by microbial carbonic anhydrase and other biological factors. *Process. Biochem.* **2010**, *45*, 1017-1021, DOI: 10.1016/j.procbio.2010.03.004.
67. Favre, N.; Christ, M.L.; Pierre, A.C. Biocatalytic capture of CO_2 with carbonic anhydrase and its transformation to solid carbonate. *J. Mol. Catal. B-Enzym.* **2009**, *60*, 163-170, DOI: 10.1016/j.molcatb.2009.04.018
68. Sánchez-Román, M.; Romanek, C.S.; Fernández-Remolar, D.C.; Sánchez-Navas, A.; Mckenzie, J.A.; Pibernat, R.A.; Vasconcelos, C. Aerobic biomineralization of Mg-rich carbonates: Implications for natural environments. *Chem. Geol.* **2011**, *281*, 143-150, DOI: 10.1016/j.chemgeo.2010.11.020.
69. Rodriguez-Blanco, J.D.; Shaw, S.; Bots, P.; Roncal-Herrero, T.; Benning, L.G. The role of Mg in the crystallization of monohydrocalcite. *Geochim. Cosmochim. Ac.* **2014**, *127*, 204-220, DOI: 10.1016/j.gca.2013.11.034.
70. Lopez-Moreno, A.; Sepulveda-Sanchez, J.; Guzman, E.; Le Borgne, S. Calcium carbonate precipitation by heterotrophic bacteria isolated from biofilms formed on deteriorated ignimbrite stones: influence of calcium on EPS production and biofilm formation by these isolates. *Biofouling* **2014**, *30*, 547-560, DOI: 10.1080/08927014.2014.888715.

71. González-Muñoz, M.T.; De Linares, C.; Martínez-Ruiz, F.; Morcillo, F.; Martín-Ramos, D.; Arias, J.M. Ca–Mg kutnahorite and struvite production by Idiomarina strains at modern seawater salinities. *Chemosphere* **2008**, DOI: 10.1016/j.chemosphere.2008.02.010.
72. Perri, E.; Tucker, M.E.; Słowakiewicz, M.; Whitaker, F.; Bowen, L.; Perrotta, I.D. Carbonate and silicate biomineralization in a hypersaline microbial mat (Mesaieed sabkha, Qatar): Roles of bacteria, extracellular polymeric substances and viruses. *Sedimentology* **2018**, *65*, 1213-1245, DOI: 10.1111/sed.12419.
73. Morgan, J.W.; Forster, C.F.; Evison, L. A comparative study of the nature of biopolymers extracted from anaerobic and activated sludges. *Water. Res.* **1990**, *24*, 743-750, DOI: 10.1016/0043-1354(90)90030-A.
74. Chen, Y.; Niu, M.; Yuan, S.; Teng, H. Durable antimicrobial finishing of cellulose with QSA silicone by supercritical adsorption. *Appl. Surf. Sci.* **2013**, *264*, 171-175, DOI: 10.1016/j.apsusc.2012.09.165.
75. Liu, Q.Y.; Zhu, J.Q.; Sun, T.; Zhou, H.Y.; Shao, Q.; Li, G.J.; Liu, X.D.; Yin, Y.S. Porphyrin nanotubes composed of highly ordered molecular arrays prepared by anodic aluminum template method. *Rsc. Advances*. **2013**, *3*, 2765-2769, DOI: 10.1039/c2ra21364h.
76. Zhou, S.X.; Chen, H.P.; Ding, C.; Niu, H.L.; Zhang, T.H.; Wang, N.F.; Zhang, Q.Q.; Liu, D.; Han, S.N.; Yu, H.G. Effectiveness of crystallitic carbon from coal as milling aid and for hydrogen storage during milling with magnesium. *Fuel* **2013**, *109*, 68-75, DOI: 10.1016/j.fuel.2012.09.002.
77. Zhou, S.X.; Chen, H.P.; Ran, W.X.; Wang, N.F.; Han, Z.Y.; Zhang, Q.Q.; Zhang, X.L.; Niu, H.L.; Yu, H.; Liu, D. Effect of carbon from anthracite coal on decomposition kinetics of magnesium hydride. *J. Alloy. Compd.* **2014**, *592*, 231-237, DOI: 10.1016/j.jallcom.2013.12.246.
78. Chen, Y.; Meng, Q.S.; Wu, M.Y.; Wang, S.G.; Xu, P.F.; Chen, H.R.; Li, Y.R.; Zhang, L.X.; Wang, L.X.; Shi, J.L. Hollow mesoporous organosilica nanoparticles: a generic intelligent framework-hybridization approach for biomedicine. *J. Am. Chem. Soc.* **2014**, *136*, 16326-16334, DOI: 10.1021/ja508721y.
79. Huang, Y.Q.; Zhao, Q.; Wang, Y.H.; Ge, S.S.; Shao, Q. A New Layered Six-Connected Network Based on Tetranuclear Copper(II) Cores. *J. Chem. Crystallogr.* **2012**, *42*, 706-710, DOI: 10.1007/s10870-012-0304-y.
80. Zhao, B.Q.; Shao, Q.; Hao, L.H. Yeast-template synthesized Fe-doped cerium oxide hollow microspheres for visible photodegradation of acid orange 7. *J. Colloid. Interf. Sci.* **2018**, *511*, 39-47, DOI: 10.1016/j.jcis.2017.09.077.
81. Huang, J.N.; Cao, Y.H.; Shao, Q.; Peng, X.F.; Guo, Z.H. Magnetic Nanocarbon Adsorbents with Enhanced Hexavalent Chromium Removal: Morphology Dependence of Fibrillar vs Particulate Structures. *Ind. Eng. Chem. Res.* **2017**, *56*, 10689-10701, DOI: 10.1021/acs.iecr.7b02835.
82. Wu, Z.J.; Gao, S.; Chen, L.; Jiang, D.W.; Shao, Q.; Zhang, B.; Zhai, Z.H.; Wang, C.; Zhao, M.; Ma, Y.Y. Electrically Insulated Epoxy Nanocomposites Reinforced with Synergistic Core–Shell SiO_2@MWCNTs and Montmorillonite Bifillers. *Macromol. Chem. Phys.* **2017**, *218*, 1700357, DOI: 10.1002/macp.201700357.
83. Chen, Y.; Han, Q.X.; Wang, Y.L.; Zhang, Q.; Qiao, X.X. Synthesis of pyridinium polysiloxane for antibacterial coating in supercritical carbon dioxide. *J. Appl. Polym. Sci.* **2015**, *132*, DOI: 10.1002/app.41723.
84. Zhao, J.k.; Ge, S.S.; Liu, L.R.; Shao, Q.; Mai, X.M.; Zhao, C.X.; Hao, L.H.; Wu, T.T.; Yu, Z.P.; Guo, Z.H. Microwave Solvothermal Fabrication of Zirconia Hollow Microspheres with Different Morphologies Using Pollen Templates and Their Dye Adsorption Removal. *Ind. Eng. Chem. Res.* **2018**, *57*, 231-241.
85. Wu, T.M.; Lin, Y.W. Doped polyaniline/multi-walled carbon nanotube composites: Preparation, characterization and properties. *Polymer* **2006**, *47*, 3576-3582, DOI: 10.1016/j.polymer.2006.03.060.
86. Liu, Q.; Zhao, Q.; Li, Y.; Wang, X. $CdCl_2$ center dot H_2O nanorods oriented parallel on the Langmuir film of (phthalocyaninato) [tetrakis (4-pyridyl) porphyrinato] cerium complex. *CrystEngComm* **2012**, 1105-1110, DOI: 10.1039/c1ce05702b.
87. Ge, S.S.; Yang, X.K.; Shao, Q.; Liu, Q.Y.; Wang, T.J.; Wang, L.Y.; Wang, X.J. Self-assembled flower-like antimony trioxide microstructures with high infrared reflectance performance. *J. Solid. State. Chem.* **2013**, *200*, 136-142, DOI: 10.1016/j.jssc.2013.01.027.
88. Liu, X.; Shao, X.Y.; Fang, G.B.; He, H.F.; Wan, Z.G. Preparation and properties of chemically reduced graphene oxide/copolymer-polyamide nanocomposites. *E-Polymers* **2017**, *17*, 3-14, DOI: 10.1515/epoly-2016-0094.
89. Tian, J.Y.; Shao, Q.; Dong, X.J.; Zheng, J.L.; Pan, D.; Zhang, X.Y.; Cao, H.L.; Hao, L.H.; Liu, J.R.; Mai, X.M.; Guo, Z.H. Bio-template synthesized NiO/C hollow microspheres with enhanced Li-ion battery electrochemical performance. *Electrochim. Acta* **2018**, *261*, 236-245, DOI: 10.1016/j.electacta.2017.12.094.
90. He, M.S.; Jin, H.; Zhang, L.L.; Jiang, H.; Yang, T.; Cui, H.Z.; Fossard, F.; Wagner, J.B.; Karppinen, M.; Kauppinen, E.I.; Loiseau, A. Environmental transmission electron microscopy investigations of Pt-Fe_2O_3

nanoparticles for nucleating carbon nanotubes. *Carbon* **2016**, *110*, 243-248, DOI: 10.1016/j.carbon.2016.09.026

91. Liu, Q.Y.; Yang, Y.T.; Li, H.; Zhu, R.R.; Shao, Q.; Yang, S.G.; Xu, J.J. NiO nanoparticles modified with 5,10,15,20-tetrakis(4-carboxyl pheyl)-porphyrin: Promising peroxidase mimetics for H_2O_2 and glucose detection. *Biosens. Bioelectron.* **2015**, *64*, 147-153, DOI: 10.1016/j.bios.2014.08.062
92. Liu, Q.Y.; Zhu, J.Q.; Shao, Q.; Fan, J.F.; Wang, D.M.; Yina, Y.S. Highly ordered arrangement of -tetrakis (4-aminophenyl) porphyrin in self-assembled nanoaggregates hydrogen bonding. *Chinese. Chem. Lett.* **2014**, *25*, 752-756, DOI: 10.1016/j.cclet.2013.12.023
93. Wu, T.H.; Shao, Q.; Ge, S.S. The facile preparation of novel magnetic zirconia composites with the aid of carboxymethyl chitosan and their efficient removal of dye. *Rsc. Advances.* **2016**, *6*, 58020-58027, DOI: 10.1039/c6ra05273h.
94. Ge, S.S.; Zhu, W.X.; Shao, Q. Fabrication and Characterization of Hollow Zirconia Microspheres Using Calcium Carbonate as Template. *Zeitschrift. für. Physikalische. Chemie.* **2016**, *230*, 1617-1628, DOI: 10.1515/zpch-2015-0681.
95. Wang, D.M.; Cao, W.B.; Fan, J. Synthesis and luminescence properties of the europium quaternary complexes nanoparticles. *Sci. China. Chem.* **2014**, *57*, 791-796, DOI: 10.1007/s11426-013-5039-x.
96. Han, Z.Z.; Sun, B.; Zhao, H.; Yan, H.X.; Han, M.; Zhao, Y.Y.; Meng, R.R.; Zhuang, D.X.; Li, D.; Ma, Y.T. Isolation of Leclercia adcarboxglata Strain JLS1 from Dolostone Sample and Characterization of its Induced Struvite Minerals. *Geomicrobiology* **2016**, *34*, 500-510, DOI: 10.1080/01490451.2016.1222469.
97. Dhami, N.K.; Reddy, M.S.; Mukherjee, A. Synergistic role of bacterial urease and carbonic anhydrase in carbonate mineralization. *Appl. Biochem. Biotech.* **2014**, *172*, 2552-2561, DOI: 10.1007/s12010-013-0694-0.
98. Favre, N.; Christ, M.L.; Pierre, A.C. Biocatalytic capture of CO_2 with carbonic anhydrase and its transformation to solid carbonate. *J. Mol. Catal. B-Enzym.* **2009**, *60*, 163-170.
99. Margesin, R.; Schinner, F. Potential of halotolerant and halophilic microorganisms for biotechnology. *Extremophiles.* **2001**, *5*, 73-83, DOI: 10.1007/s007920100184.
100. Rivadeneyra, M.A.; Delgado, G.; Ramos-Cormenzana, A.; Delgado, R. Biomineralization of carbonates by Halomonas eurihalina in solid and liquid media with different salinities: crystal formation sequence. *Res. Microbiol.* **1998**, *149*, 277, DOI: 10.1016/S0923-2508(98)80303-3.
101. Schultzelam, S.; Harauz, G.; Beveridge, T.J. Participation of a cyanobacterial S layer in fine-grain mineral formation. *J. Bacteriol.* **1992**, *174*, 7971-7981.
102. Badger, M.R.; Price, G.D. CO_2 concentrating mechanisms in cyanobacteria: molecular components, their diversity and evolution. *J. Exp. Bot.* **2003**, *54*, 609-622.
103. Smith, K.S.; Ferry, J.G. Prokaryotic carbonic anhydrases. *Fems Microbiol. Rev.* **2000**, *24*, 335-366.
104. Faridi, S.; Satyanarayana, T. Characteristics of recombinant α-carbonic anhydrase of polyextremophilic bacterium Bacillus halodurans TSLV1. *Int. J. Biol. Macromol.* **2016**, *89*, 659-668, DOI: 10.1016/j.ijbiomac.2016.05.026.
105. Dreybrodt, W.; Eisenlohr, L.; Madry, B.; Ringer, S. Precipitation kinetics of calcite in the system $CaCO_3$---H_2O---CO_2: The conversion to CO_2 by the slow process $H^+ + HCO_3^- \rightarrow CO_2 + H_2O$ as a rate limiting step. *Geochim. Cosmochim. Ac* **1997**, *61*, 3897-3904, DOI: 10.1016/S0016-7037(97)00201-9.
106. Liu, N.; Bond, G.M.; Abel, A.; Mcpherson, B.J.; Stringer, J. Biomimetic sequestration of CO_2 in carbonate form: Role of produced waters and other brines. *Fuel Process. Technol* **2005**, *86*, 1615-1625.
107. Li, W.; Chen, W.S.; Zhou, P.P.; Cao, L.; Yu, L.J. Influence of initial pH on the precipitation and crystal morphology of calcium carbonate induced by microbial carbonic anhydrase. *Colloid. Surface. B.* **2013**, *102*, 281-287, DOI: 10.1016/j.colsurfb.2012.08.042.
108. Kim, I.G.; Jo, B.H.; Kang, D.G.; Kim, C.S.; Choi, Y.S.; Cha, H.J. Biomineralization-based conversion of carbon dioxide to calcium carbonate using recombinant carbonic anhydrase. *Chemosphere* **2012**, *87*, 1091-1096, DOI: 10.1016/j.chemosphere.2012.02.003.
109. Bond, G.M.; Liu, N. Biomimetic Sequestration of CO_2 in Carbonate Form:Role of Produced Waters and Other Brines. *Prepr. Symp. Am. Chem. Soc. Div. Fuel. Chem.* **2004**, *49*, 420-421.
110. Sundaram, S.; Thakur, I.S. Induction of calcite precipitation through heightened production of extracellular carbonic anhydrase by CO_2 sequestering bacteria. *Bioresource. Technol.* **2018**, *253*, 368-371, DOI: 10.1016/j.biortech.2018.01.081.
111. Mirjafari, P.; Asghari, K.; Mahinpey, N. Investigating the Application of Enzyme Carbonic Anhydrase for CO_2 Sequestration Purposes. *Ind. Eng. Chem. Res.* **2007**, *46*, 921-926, DOI: 10.1021/ie060287u.

112. Srivastava, S.; Bharti, R.K.; Verma, P.K.; Thakur, I.S. Cloning and expression of gamma carbonic anhydrase from Serratia sp. ISTD04 for sequestration of carbon dioxide and formation of calcite. *Bioresource. Technol.* **2015**, *188*, 209-213, DOI: 10.1016/j.biortech.2015.01.108.
113. Ramanan, R.; Kannan, K.; Vinayagamoorthy, N.; Ramkumar, K.M.; Sivanesan, S.D.; Chakrabarti, T. Purification and characterization of a novel plant-type carbonic anhydrase from Bacillus subtilis. *Biotechnol. Bioproc. E.* **2009**, *14*, 32-37, DOI: 10.1007/s12257-008-0099-z.
114. Rodriguez-Blanco, J.D.; Diego, J.; Shaw, S.; Bots, P.; Roncal-Herrero, T.; Benning, L.G. The role of Mg in the crystallization of monohydrocalcite. *Geochim. Cosmochim. Ac.* **2014**, *127*, 204-220, DOI: 10.1016/j.gca.2013.11.034.
115. Ito, T. The occurrence of monohydrocalcite from calcareous sinter of cold spring of Shiowakka, Asyoro, Hokkaido. *J. Mineral. Petrol. Econ. Geol.* **1993**, *88*, 485-491.
116. Onac, B. Mineralogical studies and Uranium-series dating of speleothems from Scåri¿oara Glacier Cave (Bihor Mountains, Romania). *Theoretical & Appliedkarstology* **2001**.
117. Solotchina, E.P.; Prokopenko, A.A.; Kuzmin, M.I.; Solotchin, P.A.; Zhdanova, A.N. Climate signals in sediment mineralogy of Lake Baikal and Lake Hovsgol during the LGM-Holocene transition and the 1-Ma carbonate record from the HDP-04 drill core. *Quatern. Int.* **2009**, *205*, 38-52, DOI: 10.1016/j.quaint.2009.02.027.
118. Lowenstam, H.A. Minerals formed by organisms. *Science* **1981**, *211*, 1126-1131.
119. Señorale-Pose, M.; Chalar, C.; Dauphin, Y.; Massard, P.; Pradel, P.; Marín, M. Monohydrocalcite in calcareous corpuscles of Mesocestoides corti. *Exp. Parasitol.* **2008**, *118*, 54-58, DOI: 10.1016/j.exppara.2007.06.011.
120. Carlström, D. A crystallographic study of vertebrate otoliths. *Biol. Bull-Us.* **1963**, *125*, 441-463.
121. Catherine, H.; Skinner, W.; Osbaldiston, G.W.; Wilner, A.N. Monohydrocalcite in a guinea pig bladder stone, a novel occurrence. *Am. Mineral.* **1977**, *62*, 273-277.
122. Garvie, L.A.J. Decay of cacti and carbon cycling. *Naturwissenschaften* **2006**, *93*, 114-118, DOI: 10.1007/s00114-005-0069-7.
123. Garvie, L.A.J. Decay-induced biomineralization of the saguaro cactus (Carnegiea gigantea). *Am. Mineral.* **2003**, *88*, 1879-1888, DOI: 10.2138/am-2003-11-1231.
124. Taylor, G.F. The occurrence of monohydrocalcite in two small lakes in the South-East of South Australia. *Am. Mineral.* **1975**, *60*, 690-697.
125. Rivadeneyra, M.A.; Párraga, J.; Delgado, R.; Ramos-Cormenzana1, A.; Delgado, G. Biomineralization of carbonates by Halobacillus trueperi in solid and liquid media with different salinities. *Fems Microbiol. Ecol.* **2004**, *48*, 39-46, DOI: 10.1016/j.femsec.2003.12.008.
126. Nishiyama, R.; Munemoto, T.; Fukushi, K. Formation condition of monohydrocalcite from $CaCl_2$ –$MgCl_2$ – Na_2CO_3 solutions. *Geochim. Cosmochim. Ac.* **2013**, *100*, 217-231, DOI: 10.1016/j.gca.2012.09.002.
127. Last, F.M.; Last, W.M.; Halden, N.M. Carbonate microbialites and hardgrounds from Manito Lake, an alkaline, hypersaline lake in the northern Great Plains of Canada. *Sediment. Geol.* **2010**, *225*, 34-49, DOI: 10.1016/j.sedgeo.2010.01.006.
128. Stoffers, P.; Fischbeck, R. Monohydrocalcite in the sediments of Lake Kivu (East Africa). *Sedimentology* **1974**, *21*, 163-170, DOI: 10.1111/j.1365-3091.1974.tb01787.x.
129. Taylor, G.F. The occurrence of monohydrocalcite in two small lakes in the southeast of South Australia. *Amer Mineral* **1975**, *60*, 690-697.
130. Zhang, Y.; Dawe, R.A. Influence of Mg^{2+} on the kinetics of calcite precipitation and calcite crystal morphology. *Chem. Geol.* **2000**, *163*, 129-138, DOI: 10.1016/S0009-2541(99)00097-2
131. Davis, K.; Dove, P.; De Yoreo, J. The role of Mg^{2+} as an impurity in calcite growth. *Science* **2000**, *290*, 1134-1137, DOI: 10.1126/science.290.5494.1134.
132. Moomaw, A.S. The unique nature of Mg^{2+} channels. *Physiology* **2008**, *23*, 275-285, DOI: 10.1152/physiol.00019.2008.
133. Mucci, A.; Morse, J.W. The incorporation of Mg^{2+} and Sr^{2+} into calcite overgrowths: influences of growth rate and solution composition. *Geochim. Cosmochim. Ac* **1983**, *47*, 217-233.
134. Fukushi, K.; Suzuki, Y.; Kawano, J.; Ohno, T.; Ogawa, M.; Yaji, T.; Takahashi, Y. Speciation of magnesium in monohydrocalcite: XANES, ab initio and geochemical modeling. *Geochim. Cosmochim. Ac* **2017**, *213*, 457-474, DOI: 10.1016/j.gca.2017.06.040.

135. Ludi, B.; Niederberger, M. Zinc oxide nanoparticles: chemical mechanisms and classical and non-classical crystallization. *Dalton. T.* **2013**, *42*, 12554-12568, DOI: 10.1039/c3dt50610j.
136. Morse, J.W.; Given, R.K.; Wilkinson, B.H. Kinetic control of morphology, composition, and mineralogy of abiotic sedimentary carbonates; discussion and reply. *Science* **1985**, *55*, 109-119.
137. Fernández-Díaz, L.; Putnis, A.; Prieto, M.; Putnis, C.V. The role of magnesium in the crystallization of calcite and aragonite in a porous medium. *Journal of Intercultural Studies* **1996**, *15*, 73-84.